Charles University

Faculty of Science

Study program: Chemie

Branch of study: Biofyzikální chemie (NBIOFYZD)

Bc. David Gücklhorn

Tracking membrane permeabilization on single lipid vesicles - method development.

Sledování permeabilizace membrány na jednotlivých lipidových vezikulech - vývoj metody.

Diploma thesis

Supervisor: RNDr. Radek Šachl Ph.D.

Prague, 2022

Prohlášení:

Prohlašuji, že jsem závěrečnou práci zpracoval/a samostatně a že jsem uvedl/a všechny použité informační zdroje a literaturu. Tato práce ani její podstatná část nebyla předložena k získání jiného nebo stejného akademického titulu.

V Praze, 26.8.2022

Podpis:

Acknowledgements:

Firstly, I would like to thank my supervisor RNDr. Radek Šachl Ph.D. for competent supervision, good advice and patience during the initial struggles in the development of this method.

I would also like to thank Sabína Macharová Ph.D. for teaching me the basics of electroformation and helping me in the beginning of my experiments. I am also grateful to Peter Kapusta Ph.D. for his instructions in confocal microscopy. My gratitude also belongs to Petra Riegerová Ph.D. for allowing me to present her unpublished results in the thesis. I am also grateful to MSc. Vandana Singh for being always available for trouble-shooting experimental problems and consultation.

Lastly, I would like thank prof. Walter Nickel and his group from Heidelberg University Center, Germany, for providing me with FGF2 proteins.

Abstract:

Protein complexes are challenging systems to study, especially when these complexes form on lipid membranes only for a short period of time. This is also the case of fibroblast growth factor 2 (FGF2), a protein that has many physiological and pathological functions in the human organism. It plays major role in the development of cancer as it promotes cell survival and angiogenesis. It also serves as a basis for development of novel treatments of nerve injuries. Despite being heavily studied for many years, it remains unclear how the protein is translocated into the extracellular space where it performs its function.

To study complex systems such as FGF2 that self-assembles on the membrane into membrane penetrating pores we decided to develop a simple and efficient fluorescent microscopy method. This method is called double leakage single GUV assay (DLSGA). It utilizes giant unilamellar vesicles (GUVs) mimicking native cellular membranes. In a single experiment, up to 300 individual GUVs are imaged for the content of a leakage dye that reports on the presence of FGF2 pores. During three measurements and under different conditions, detailed information about pore-opening dynamics is gained for each GUV. Results of these measurements are then used to divide GUVs into six groups based on formation and stability of FGF2 pores. This approach thus allows for getting deeper insight into the mechanism of FGF2 translocation across the membrane.

More specifically, by using this method, we were able to confirm the role of Y81 in hastening insertion of FGF2 oligomers into the membrane. We were also able to observe differences in the formation of FGF2 pores by distinct FGF2 variants with mutated cysteines. This turned out to be interesting in conjunction with the results that were previously obtained by complementary methods. Dual-color FCS and TIRF microscopy experiments revealed that C77-C77 disulfide bridges serve to form FGF2 dimers whereas C95-C95 disulfide bridges facilitate formation of higher oligomeric states. It is speculated that these dimers represent crucial intermediates in the formation of higher oligomers that are ultimately responsible for translocation across membrane. Our experiments revealed that FGF2 with mutated C95 (which can only form dimers) is able to form stable pores to a similar degree as the wild type variant of the protein. This experiment thus confirms that dimers as well as the higher oligomer species insert efficiently into the membrane and underpin the importance of dimers for translocation of the protein.

Importantly, by conducting DLSGA experiments with 4 KDa large fluorescent dyes we were able to estimate the diameter of FGF2 pores at 2.34 nm. These experiments also showed that GFP, which is commonly used as a fluorescent tag of many proteins, increases the size of FGF2 pores.

Abstrakt:

Proteinové komplexy se obtížně studují, obzvlášť pokud vznikají jen v membránovém prostředí a na velmi krátkou dobu. Toto je problematické například v případě fibroblastového růstového faktoru 2 (FGF2), což je protein s mnoha fyziologickými i patologickými funkcemi v lidském organismu. Hraje zásadní roli v rozvoji různých nádorových onemocnění, protože braní apoptóze buněk pomocí autokrinní signalizace a také stimuluje angiogenezi. Zároveň je v současné době zkoumána možnost jeho uplatnění v léčbě zranění periferního nervstva. Přestože je důkladně zkoumán již řadu let, mechanismus jeho translokace do mezibuněčného prostoru, kde vykonává svou funkci, nebyl zcela objasněn.

Pro studium komplexních systému, jako jsou membránové póry tvořené FGF2, jsme vyvinuli jednoduchou a efektivní metodu fluorescenční mikroskopie. Tato metoda se jmenuje dvojitá permeabilizační esej jednotlivých vezikulů (DLSGA). Využívá lipidové vezikuly (GUVs) pro simulaci buněčné membrány. V jediném experimentu je možné sledovat až 300 jednotlivých vezikulů a tvorbu pórů v jejich membráně. Během třech měření za různých podmínek získáváme detailní informaci o dynamice otevírání pórů na každém vezikulu. Na základě těchto měření je možné jednotlivé vezikuly rozdělit do šesti skupin podle toho, jestli se na nich tvořili póry a jak byly dané póry stabilní. Tento přístup umožňuje získat hlubší porozumění mechanismu translokace FGF2 přes buněčnou membránu.

Konkrétně se nám podařilo potvrdit roli Y81 v urychlování inserce FGF2 oligomerů do membrány. Navíc jsme pozorovali rozdíl v tvorbě pórů u variant s mutovanými cysteiny. Výsledky pro cysteinové mutanty jsou velmi zajímavé v kombinaci se zjištěnými oligomerizačními stavy těchto mutantů, které byly získány pomocí Dual-color FCS. Ukázalo se, že C77-C77 disulfidový můstek slouží ke tvorbě FGF2 dimerů, zatímco C95-C95 můstek umožňuje tvorbu vyšších oligomerizačních stavů. Experimenty pomocí TIRF mikroskopie ukázaly, že dimery FGF2 hrají klíčovou roli v mechanismu translokace FGF2 přes membránu. Spekuluje se, že tyto dimery jsou meziprodukty pro tvorbu vyšších oligomerů, které se záhy poté translokují přes membránu. Experimenty v této práci ukazují, že C95A mutant, který dokáže vytvářet pouze dimery, je schopen vytvářet stabilní póry do podobné míry jako nemutované varianty. To znamená, že pro zanoření FGF2 do membrány není potřeba vyšších oligomerizačních stavů, které toho jsou ale také schopny.

Díky sérii DLSGA experimentů za použití 4 KDa dextranových fluorescenčních barev se podařilo odhadnout průměr FGF2 pórů na 2,34 nm. Tyto experimenty také ukázaly, že GFP, které se často využívá pro tvorbu fluorescenčních fúzních proteinů, zvyšuje velikost FGF2 pórů.

Contents:

1. Abbreviations

Standard 1-letter aminoacid abbreviations were used

bFGF	basic fibroblast growth factor
BSA	bovine serum albumin
Chol	cholesterol
DLSGA	double leakage single GUV assay
DNA	deoxyribonucleic acid
DOPE	1,2-dioleoyl-sn-glycero-3-phosphoethanolamine
ER	endoplasmic reticulum
FGF2	fibroblast growth factor 2
FITC	fluorescein isothiocyanate
FRAP	fluorescence recovery after photobleaching
FRET	Förster resonance energy transfer
GFP	green fluorescent protein
GUV	giant unilamellar vesicle
HEPES	4-(2-hydroxyethyl)-1-piperazineethanesulfonic acid)
HMW	high molecular weight
HOMO	highest occupied molecular orbital
IC	internal conversion
ISC	inter-system crossing
LMW	low molecular weight
LUMO	lowest unoccupied molecular orbital
PC	phosphatidylcholine
PC10	phosphatydilcholine based lipid composition with 10% PIP_2

pCMF	unnatural amino acid p-carboxylmethylphenylalanine
PE	phosphatidylethanolamine
PI	phosphatidylinositol
PIP_2	L-α-phosphatidylinositol-4,5-bisphosphate
PM2	plasma-like membrane lipid composition with 2% PIP_2
PM5	plasma-like membrane lipid composition with 5% PIP_2
PS	phosphatidylserine
RNA	ribonucleic acid
RT	room temperature
TRITC	Tetramethylrhodamine isothiocyanate
VIS	visible part of electromagnetic radiation spectrum
WT	wild type

2. Introduction

In this thesis a fluorescence microscopy method was developed and used to study protein (FGF2) which binds to cellular membrane, then oligomerizes and forms membrane pores. Fluorescence basics are explained in the following chapters for better understanding of the method that was developed. The method was used specifically to study FGF2 translocation mechanism across cellular membrane. For this reason a chapter that is dedicated to this protein is also included with emphasis on current state of knowledge about the aforementioned translocation mechanism.

2.1. Fluorescence

Emission of ultraviolet, visible or infrared light from an excited source that is not solely conditioned by the rise in temperature is called luminescence. There are many types of luminescence based on the source of excitation (**Table 1**).

Table 1. Various types of luminescence and their respective sources of excitation. *Taken and modified from (1).*

TYPE OF LUMINESCENCE	SOURCE OF EXCITATION
Photoluminescence (fluorescence, phosphorescence, delayed fluorescence)	Absorption of light (photons)
Radioluminescence	Ionizing radiation
Cathodoluminescence	Cathode rays (electron beams)
Electroluminescence	Electric field
Thermoluminescence	Heating after prior storage of energy
Chemiluminescence	Chemical process
Bioluminescence	Biochemical process
Triboluminescence	Frictional and electrostatic forces
Sonoluminescence	Ultrasounds

Photoluminescence is caused by absorption of photons by fluorophores. The most common type of photoluminescence is fluorescence. The process of fluorescence consists of three main steps which all happen at a different timescale. Firstly, absorption of a photon leads to the excitation of an electron from the highest occupied molecular orbital (HOMO) to the lowest unoccupied molecular orbital (LUMO). According to the Boltzmann distribution, this transition will mostly happen from the lowest vibrational state of the ground state. This state is the most populated

state at room temperature and has a specific internuclear distance. The transition happens on a femtosecond timescale (10^{-15} s). Movement of nuclei happens on significantly slower timescale (10^{-13} s), therefore, the internuclear distance cannot be adjusted during the electronic transition. For this reason, the most likely transitions are vertical transitions on the energy – internuclear distance plot (**Figure 1**); this is known as the Franck-Condon principle (2,3). Consequently, as transitions happen mostly from the lowest vibrational state of the ground electronic state, it is likely to be into a higher vibrational state (vibrational state with which there is the greatest overlap of the vibrational wave function). (4)

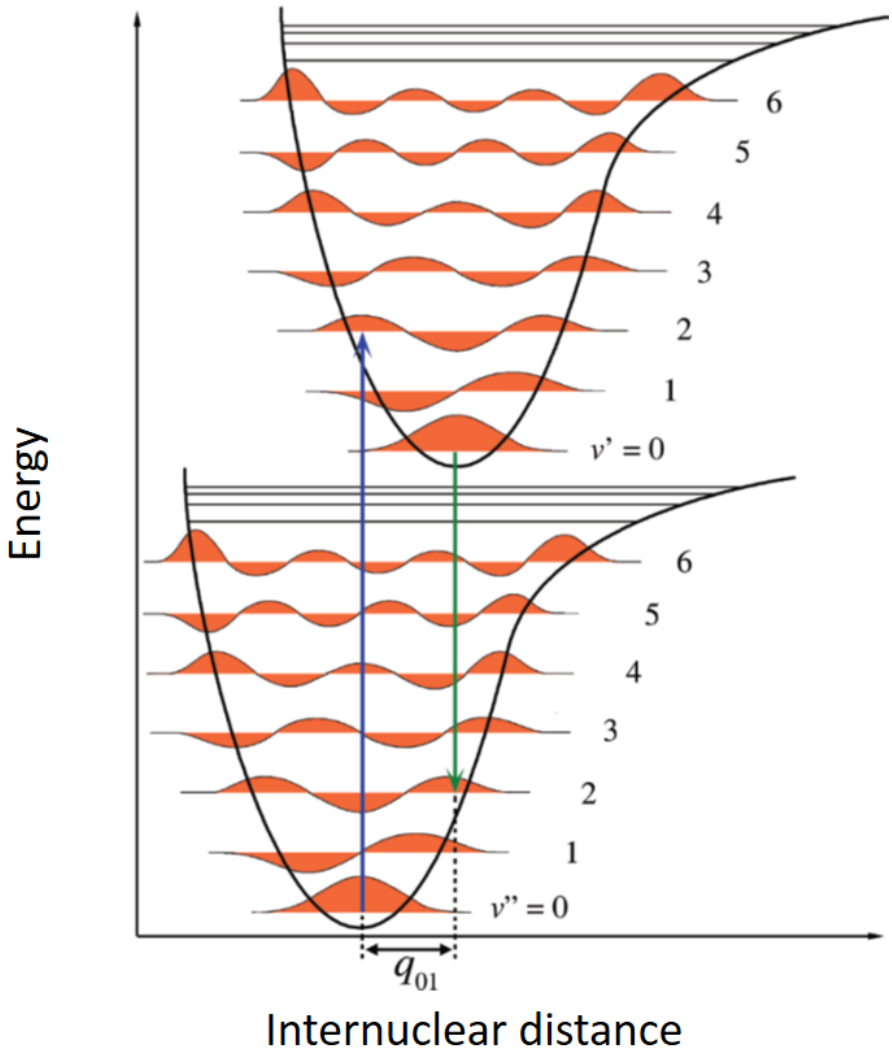

Figure 1. Graphical representation of the Franck-Condon principle. *Energy of electronic states is represented by thick black lines. Vibrational states are represented by their potential energy curves (thin black lines with orange areas). Blue arrow represents excitation while green arrow represent return to electronic ground state by photon emission. Taken and modified from (5).*

Secondly, since excitation into higher vibrational states is preferred, another process occurs to dissipate this energy – vibrational relaxation. Vibrational relaxation to the lowest vibrational state of the excited electronic state (Kasha's rule) occurs at the picosecond timescale (10^{-12} s). (6)

Lastly, the energy of the excited state is released in the form of photon emission occurring at the nanosecond timescale (10^{-9} s). Franck-Condon principle applies to both absorption and emission of photons. This means that when molecules return to the electronic ground state by emission it is into higher vibrational states. Due to this fact and the vibrational relaxation which occurred beforehand, the energy of the emitted photon is lower than that of the absorbed photon. This results in a shift towards a longer emission wavelength. The greatest probability of the transition is for the vibrational states that have the greatest overlap between the vibrational wave functions. Multiple different transitions are possible, which gives absorption and emission spectra its characteristic shape (**Figure 2**). Additionally, differences between vibrational levels are similar in both ground and excited states, which makes the absorption spectra look like a mirror image of the emission spectra (1). The gap (in wavenumbers) between the absorption and emission maximum is called the Stokes shift (7).

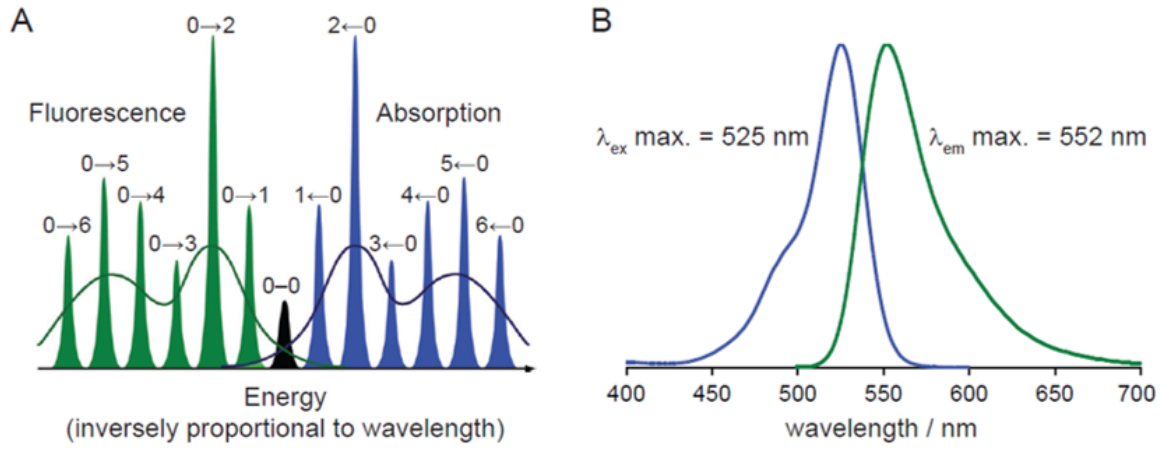

Figure 2. A: *Schematic representation of the absorption and fluorescence spectra. Electronic transitions between the lowest vibrational levels of the electronic states (the 0-0 transition) have the same energy in both absorption and fluorescence.* ***B:*** *Spectrum of a commonly used fluorescent dye, Rhodamine 6G. Taken from (5).*

2.2. Perrin – Jablonski diagram

Once a fluorophore is excited to the first excited singlet state, S_1, it can release the excess energy and return to the ground state S_0 either via emission of a photon or by non-radiative means.

Some of these processes and relationships between them are shown in Perrin – Jablonski diagram (**Figure 3**).

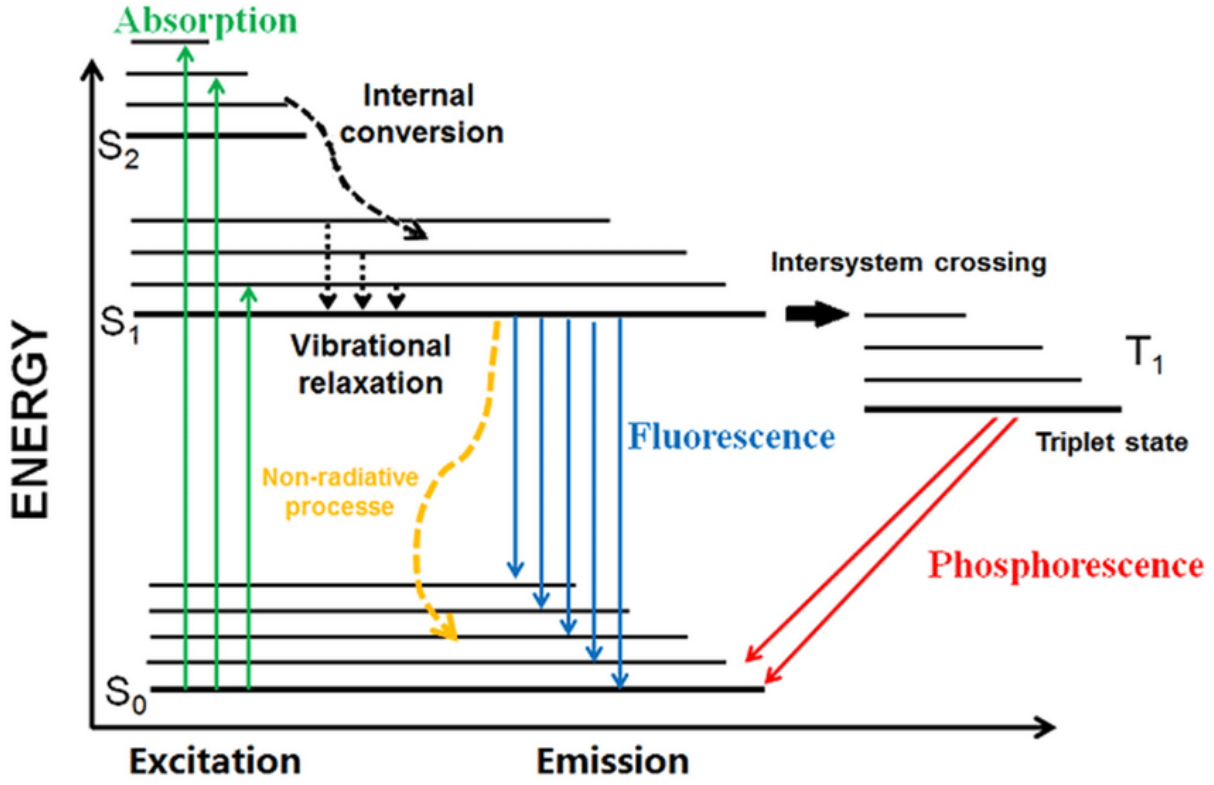

Figure 3. Perrin – Jablonski diagram. *Schematic representation of various different processes that occur after electron excitation of a fluorophore. Taken from (8).*

One method of non-radiative deexcitation is internal conversion (IC). It can occur between two electronic states of the same multiplicity when their vibrational states have similar energy. It is a lot more efficient between S_2 and S_1 states than S_1 and S_0 states because of a smaller energy gap between S_2 and S_1 states. This way, excess energy is released as heat by vibrational relaxation.

Intersystem crossing (ISC) is a spin-forbidden transition between singlet and triplet states and occurs due to spin-orbit coupling – a coupling between the orbital magnetic moment and spin magnetic moment. Presence of heavy atoms increases spin-orbit coupling which in turn increases the likelihood of ISC. (9–11) It is also influenced by paramagnetic species (12). Its efficiency also depends on the rate constants for other pathways of deexcitation:

$$k_D = k_r + k_{IC} + k_{ISC} = k_r + k_{nr} = \frac{1}{\tau}, \quad (1)$$

where k_D is the rate constant of deexcitation, k_r the rate constant of radiative deexcitation, k_{IC} the rate constant of internal conversion, k_{ISC} the rate constant of intersystem crossing, k_{nr} the rate constant of non-radiative deexcitation and τ is the excited state lifetime. Other ways of non-radiative deexcitation include intramolecular charge transfer and conformational change. (1)

As for the radiative deexcitation, there are a couple of options. Most common is fluorescence which is the release of excess energy via emission of photons.

Phosphorescence is a process during which photon is emitted as a result of $T_1 \rightarrow S_0$ transition. This process is also forbidden and therefore happens on longer timescales than fluorescence (μs - minutes). The lowest vibrational state of triplet state T_1 has lower energy than the lowest vibrational state of the first excited singlet state S_1. For this reason the energy of the emitted photon is smaller than would be the energy of photon emitted by fluorescence. This results in a shift towards longer wavelengths of the photon emitted by phosphorescence.

There are more ways of photon emission that are dependent on the triplet state. Thermally activated delayed fluorescence (also known as E-type delayed fluorescence because it was first observed in eosin) happens after the reverse intersystem crossing $T_1 \rightarrow S_1$ when the energy difference between these two states is small. (13,14) Spectral distribution of this phenomena is the same as for fluorescence as the deexcitation happens from S_1 state, however, this type of fluorescence has a much longer decay time constant. As it is thermally activated, its efficiency increases with temperature. It is very efficient in fullerenes (1).

Another kind of delayed fluorescence that is also triplet dependent is called triplet-triplet annihilation (also known as P-type delayed fluorescence because it was first observed with pyrene). It can occur in concentrated solutions when two molecules in triplet state collide. This can provide enough energy to push one of these molecules into S_1 state. The decay time constant is half of the lifetime of the triplet state in dilute solution. Due to the mechanism, the fluorescence intensity has quadratic dependence on excitation light intensity. (1)

A molecule in the triplet state can also undergo triplet-triplet transition into higher excited triplet state by absorption of a photon with suitable energy.

2.3. Fluorescence lifetime and quantum yield

The most important spectral properties of fluorophores include excitation and emission wavelengths, lifetime of excited state and quantum yield.

Excited state lifetime is a measure of how quickly a molecule is deexcited. To show some basic equations that describe excited state lifetime mathematically, let us have this situation: a dilute solution of fluorophore molecules A that are irradiated by a very short pulse of excitation light. This brings some molecules A from the singlet ground state S_0 to the first excited singlet state S_1. These molecules then undergo radiative or non-radiative deexcitation. The rate of disappearance of excited molecules can be expressed using classical chemical kinetics as:

$$-\frac{d[A^*]}{dt} = (k_r + k_{nr})\,[A^*] \tag{2}$$

Concentration of molecules in the first excited singlet state is represented as *[A*], t* represents time, k_r is the rate constant of radiative deexcitation and k_{nr} is the rate constant of non-radiative deexcitation from the first excited singlet state. Integration of equation (2) leads to:

$$[A^*] = [A^*]_0 \exp\left(-\frac{t}{\tau_S}\right) \tag{3}$$

The concentration of fluorophores in the first excited singlet state at time 0 (right the pulse of excitation light ended and before any of these molecules deexcited) is represented as $[A^*]_0$; τ_S represents the lifetime of the first singlet excited state which is inversely proportional to the rate constants of deexcitation:

$$\tau_S = \frac{1}{(k_r + k_{nr})} \tag{4}$$

Fluorescence intensity can be defined as the amount of photons emitted per unit time and per unit volume of a solution. Fluorescence intensity at time after excitation pulse, *I(t)*, is proportional to the concentration of fluorophores in the first singlet excited state and the rate of radiative deexcitation from this state:

$$I(t) = k_r[A^*] = k_r[A^*]_0 \exp\left(-\frac{t}{\tau_S}\right) \tag{5}$$

Fluorescence quantum yield, Φ_F, is the fraction of fluorophore molecules in first excited singlet state that undergo return to the singlet ground state S_0 by fluorescence:

$$\Phi_F = \frac{k_r}{k_r + k_{nr}} = k_r \tau_S \quad (6)$$

Similarly, quantum yield of the intersystem crossing, Φ_{ISC}, can be mathematically described as:

$$\Phi_{ISC} = \frac{k_{ISC}}{k_r + k_{nr}} = k_{ISC} \tau_S \quad (7)$$

The rate constant of intersystem crossing is represented as k_{ISC}. The quantum yield of phosphorescence, Φ_P, can described as:

$$\Phi_P = \frac{k_r^T}{k_r^T + k_{nr}^T} \Phi_{ISC}, \quad (8)$$

where the rate constant of radiative deexcitation from the triplet state to the singlet state is represented by k_r^T and the rate constant of non-radiative deexcitation from the triplet state to the singlet state is represented as k_{nr}^T.

2.4. Fluorescence quenching

In a condensed phase, there are many more ways of non-radiative deexcitation due to intermolecular interactions. Such ways are: electron transfer, proton transfer, energy transfer, excimer or exciplex formation. (15) These deexcitation pathways may compete with fluorescence emission if they take place on a timescale comparable to the lifetime of excited state. (1)

Fluorescence is known to be quenched by halogen anions (16), charge transfer has been proposed to be the quenching mechanism (17).

Förster resonance energy transfer (FRET) happens over short distances (10 nm) through dipole-dipole coupling. (18) Its efficiency is influenced by spectral overlap of donor emission spectra and acceptor absorption spectra, the distance between a donor and an acceptor and relative orientation of their respective emission and absorption dipole moments. It is heavily utilized because of the distance dependency as can be used to determine the structure of biomolecules or interactions between them (19–23). It can also be used to determine some otherwise almost inaccessible parameters such as the size of lipid nanodomains (24).

As mentioned above, presence of heavy atoms enhances the efficiency of intersystem crossing due to the increase in spin-orbit coupling, which in turn makes the change of multiplicity easier ($S_1 \rightarrow T_1$). As intersystem crossing is an alternative deexcitation pathway to fluorescence, its increase leads to quenching. This is true for both internal heavy atoms (part of the structure of a fluorophore) (25,26) and external heavy atoms (in solution or in other molecules close by) (10,27).

Molecules of fluorophores at high concentrations are prone to aggregation, especially when being in aqueous solutions. This can lead to quenching (17,28–31), as the aggregation decreases fluorescent intensity and changes the fluorescence spectra by enhancing shorter-wavelength components of the emission spectra.

The characteristics of fluorescence (spectrum, quantum yield, lifetime) are affected by any excited state process involving interactions of the excited molecule with its close environment. Due to many factors that influence fluorescence quenching and the timescale at which this influence can be manifested (excited state lifetime), fluorescence quenching is ideal to study structure and dynamics of biomolecules such as proteins (32–34) and nucleotides (35–39).

It should be noted that some excited-state processes (conformational change, electron transfer, proton transfer, energy transfer, excimer or exciplex formation) may lead to fluorescent species whose emission may be superimposed over that of the initially excited molecule. Such an emission should be distinguished from the 'primary' fluorescence arising from the excited molecule. (1)

2.5. Effect of temperature

An increase in temperature results in a decrease in the fluorescence quantum yield and the lifetime because most non-radiative processes have increased efficiency at higher temperature. Experiments revealed a simple empirical relationship between fluorescence quantum yield, Φ_F, and thermodynamic temperature, T:

$$\ln\left(\frac{1}{\Phi_F - 1}\right) = \frac{1}{T} \tag{7}$$

The effect of temperature is even more pronounced for phosphorescence because the triplet states are very efficiently deactivated by collisions with solvent molecules (or oxygen and impurities) due to their longer lifetime. These effects can be reduced and may even disappear

when the molecules are in a frozen solvent, or in a rigid matrix (e.g. polymer) at room temperature. The increase in phosphorescence quantum yield by cooling can reach a factor of 10^3, whereas this factor is generally no larger than 10 or so for fluorescence quantum yield. (1)

In condensed phase, there many more parameters that can affect the quantum yields and lifetimes: pH, polarity, viscosity, hydrogen bonding, presence of quenchers, etc. (1)

2.6. Photobleaching

Photobleaching is irreversible degradation of fluorophores. It happens as a result of a reaction of excited fluorophore with other molecules such as oxygen. There are big differences between various fluorophores and their resistance to photobleaching. Some fluorophores can undergo millions of excitation–emission cycles while others are photobleached only after a couple of cycles. Photobleaching has been heavily studied because it undesirably influences various fluorescence techniques (40–45).

There are multiple known mechanisms of photobleaching. Typically, the triplet state of fluorophores is involved as it has significantly longer lifetime than the excited singlet state and also has unpaired electrons which makes it quite reactive. (5) Oxygen concentration is a very important factor when it comes to photobleaching because it facilities $T_1 \rightarrow S_0$ transitions, serving as triplet state quencher (46–48). This, however, leads to formation of reactive oxygen species which can then chemically modify fluorophores such as aminoacids or nucleic acid bases (49,50). Photobleaching can be mitigated by including efficient triplet state quenchers in solution to prevent formation of reactive oxygen species (51–53).

Fluorescence recovery after photobleaching (FRAP) utilizes photobleaching to study systems where diffusion of fluorophores is limited, such as membrane systems (54–58). This method is widely used to study biological systems. First, the selected sample area is quickly irradiated by excessive amount of excitation light. This results in photobleaching of all fluorophores in the area. Then, fluorescence from that area is being recorded as it is recovered with diffusion of functional molecules of fluorophores. **Figure 4** shows schematic illustration of this method which was used to study integrins.

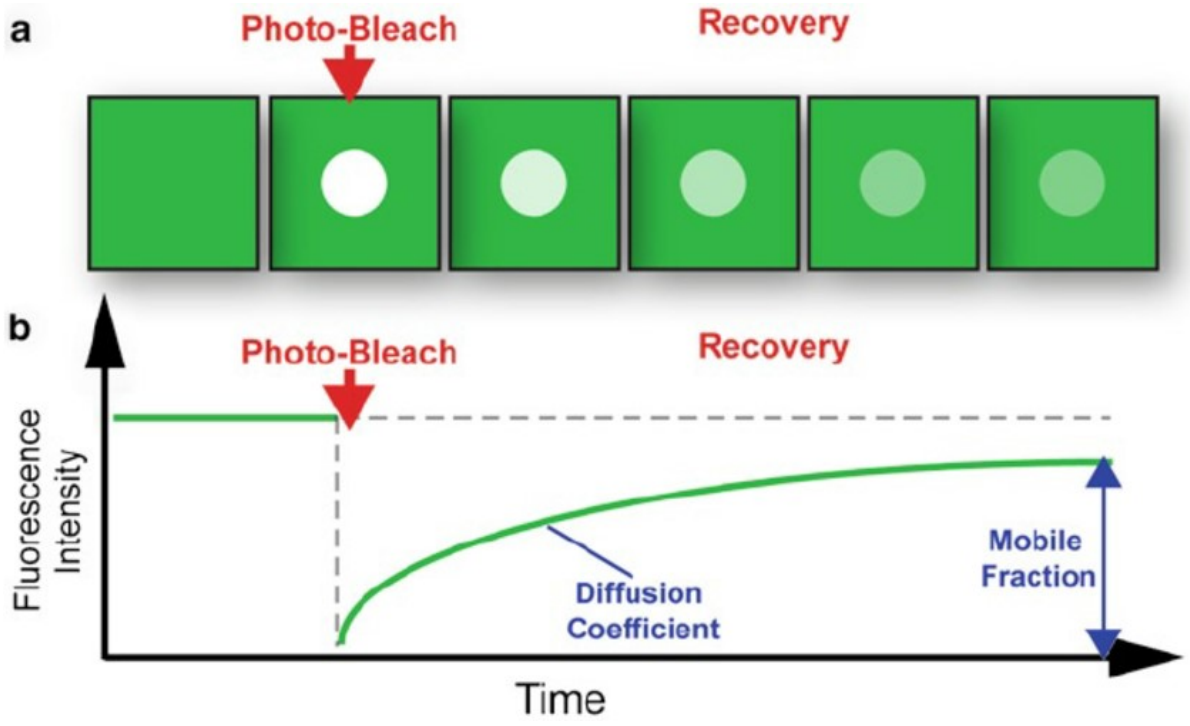

Figure 4. Schematic illustration of fluorescence recovery after photobleaching method. *A: irraditated area is photobleached and then recovers its fluorescence with diffusion of functional fluorophore molecules.* ***B:*** *kinetics of recovery provides information about diffusion coeficient and about fraction of immobile molecules if fluorescence does not recover completely. Taken from (58).*

2.7. Fluorophores

As mentioned above, fluorophores are molecules that enter the excited singlet state by absorbing the energy of photons. In order to return to the ground state, these molecules then emit photons with lower energy than they absorbed. The energy of emitted photons should preferably correspond to the VIS part of the electromagnetic radiation spectrum. Organic compounds which only contain σ (sigma) bonds usually require absorption of photons at wavelengths below 160 nm to enter the excited state. Unfortunately, energy of such photons is high enough to cause photochemical decomposition of irradiated molecules. Double or triple bonds are composed of σ and π (pi) bonds. For molecules that contain π bonds, the electronic transition with the smallest energy gap is typically bonding π orbital → antibonding π^* orbital. (59) The energy gap between these two states corresponds to photons with the wavelength of 170 nm for a molecule containing one double or triple C-C bond. Double bonds that are separated by one single bond (conjugated double bonds) share energy of their π electrons which in turn reduces the energy gap for bonding π orbital → antibonding π^* orbital transition. By increasing the number of conjugated double bonds, the excitation wavelength can be shifted to the VIS part of the electromagnetic radiation spectrum. (60)

When a heteroatom is involved in the system of conjugated double bonds the electronic transition with the smallest energy gap can be nonbonding n orbital → antibonding π^* orbital. These transitions have at least 100 times smaller molar absorption coefficients than $\pi \rightarrow \pi^*$ and a proportionally smaller radiative deexcitation rate constant. These two factors result in very weak fluorescence caused by these transitions and a very low fluorescence quantum yield. (1)

Examples of common fluorescent probes – fluorophores that are used for fluorescent experiments to study physicochemical, biochemical and biological systems (1) – can be found in **Figure 5**.

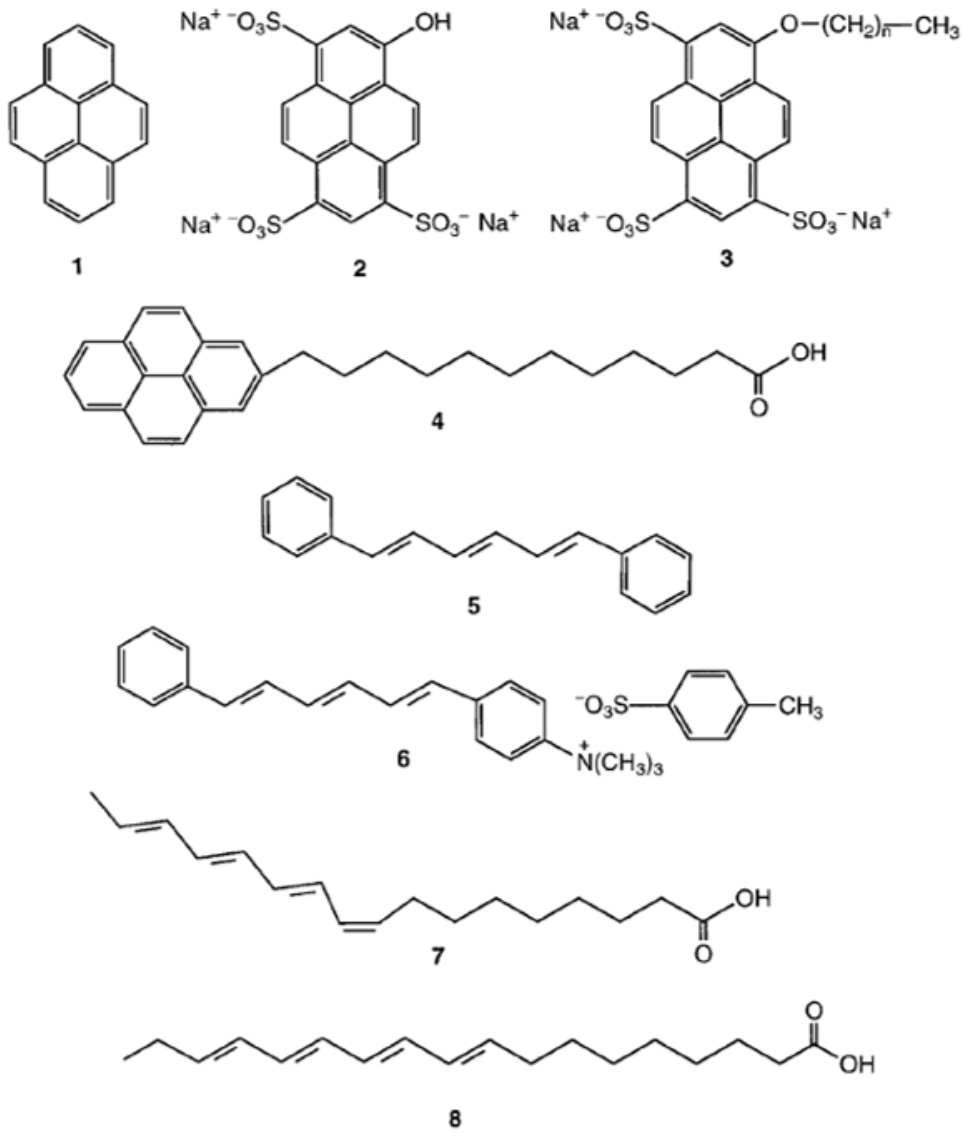

Figure 5. Examples of common fluorophores. 1: *pyrene.* ***2:*** *8-hydroxypyrene-1,3,6-trisulfonic acid trisodium salt (pyranine).* ***3:*** *8-alkoxypyrene-1,3,6-trisulfonic acid trisodium salt.* ***4:*** *1-pyrenedodecanoic acid.* ***5:*** *1,6-diphenyl-1,2,5-hexatriene (DPH).* ***6:*** *1-(4-trimethylammoniumphenyl)-6-phenyl-1,3,5-hexatriene, p-toluene sulfonate (TMA–DPH).* ***7:*** *cis-parinaric acid.* ***8:*** *trans-parinaric acid. Taken from (1).*

2.8. Research applications of fluorescence

Fluorescence is widely utilized in research for three main reasons. First reason is that fluorescence can be measurably influenced by many factors, therefore, with a clever experiment design, fluorescence can be used to study wide variety of systems and wide variety of properties of the respective systems. Second reason is that fluorescence is highly sensitive (detectors nowadays can detect single photons) and specific (signal originates only from molecules of fluorophores that are excitable by the used excitation source). Third reason is that fluorescence happens on the nanosecond timescale and detectors are capable of resolving such fast events, which makes fluorescence perfect to study processes which happen on this timescale (many biological processes) that would otherwise be difficult to study. Examples of utilization of fluorescent probes can be found in **Table 2.**

Table 2. Examples of utilization of fluorescent probes in various research fields. *Taken from (1).*

Research field	Accessible information with a use of fluorescent probes
Polymers	dynamics of polymer chains; microviscosity; free volume; orientation of chains in stretched samples; miscibility; phase separation; diffusion of species through polymer networks; end-to-end macrocyclization dynamics; monitoring of polymerization; degradation
Solid surfaces	nature of the surface of colloidal silica, clays, zeolites, silica gels, porous Vycor glasses, alumin a: rigidity, polarity and modification of surfaces
Surfactant solutions	critical micelle concentration; distribution of reactants among particles; surfactant aggregation numbers; interface properties and polarity; dynamics of surfactant solutions; partition coefficients; phase transitions; influence of additives
Biological membranes	fluidity; order parameters; lipid–protein interactions; translational diffusion; site accessibility; structural changes; membrane potentials; complexes and binding; energy-linked and light induced changes; effects of additives; location of proteins; lateral organization and dynamics

Vesicles	characterization of the bilayer: microviscosity, order parameters; phase transition; effect of additives; internal pH; permeability
Proteins	binding sites; denaturation; site accessibility; dynamics; distances; conformational transition
Nucleic acids	flexibility; torsion dynamics; helix structure; deformation due to intercalating agents; photocleavage; accessibility; carcinogenesis
Living cells	visualization of membranes, lipids, proteins, DNA, RNA, surface antigens, surface glycoconjugates; membrane dynamics; membrane permeability; membrane potential; intracellular pH; cytoplasmic calcium, sodium, chloride, proton concentration; redox state; enzyme activities; cell–cell and cell–virus interactions; membrane fusion; endocytosis; viability, cell cycle; cytotoxic activity
Fluoroimmunochemistry	fluoroimmunoassays

2.9. Fluorescence microscopy

Perhaps the most common application of fluorescence is fluorescence microscopy. In classical optical microscopy, a light source is used to irradiate a sample and detect photons that it reflects. In fluorescence microscopy a light source with specific wavelength is used for excitation. The spatial resolution of optical microscopy is limited by the diffraction limit of visible light (half of wavelength of light detected by the microscope detector) and is deteriorated by out-of-focus photons which blur the image. (1)

There are several techniques that have been developed recently that surpass the diffraction limit (61–64). These so–called super–resolution or nanoscopy techniques utilize many different principles and are suitable for different applications. The method developed in this thesis utilize is based on laser scanning confocal fluorescence microscopy and so it will be the main focus of this chapter.

2.9.1. Laser scanning confocal fluorescence microscopy

Confocal fluorescence microscopy utilizes a set of two pinholes (**Figure 6**). The first pinhole serves to focus excitation light to a very small volume (10^{-15} l). The second pinhole prevents

collection of emitted out-of-focus photons thus limiting depth of field and also greatly reducing background. This enables detection of photons from slices of defined thickness allowing for construction of 3D image of the measured sample (65–67). Image is recorded by scanning the sample with highly focused laser beam utilizing a scanning stage with very precise movement. At the same time, this is also a disadvantage of confocal microscopy as compared to conventional wide-field microscopy which can give information about much larger part of the sample at a time.(68)

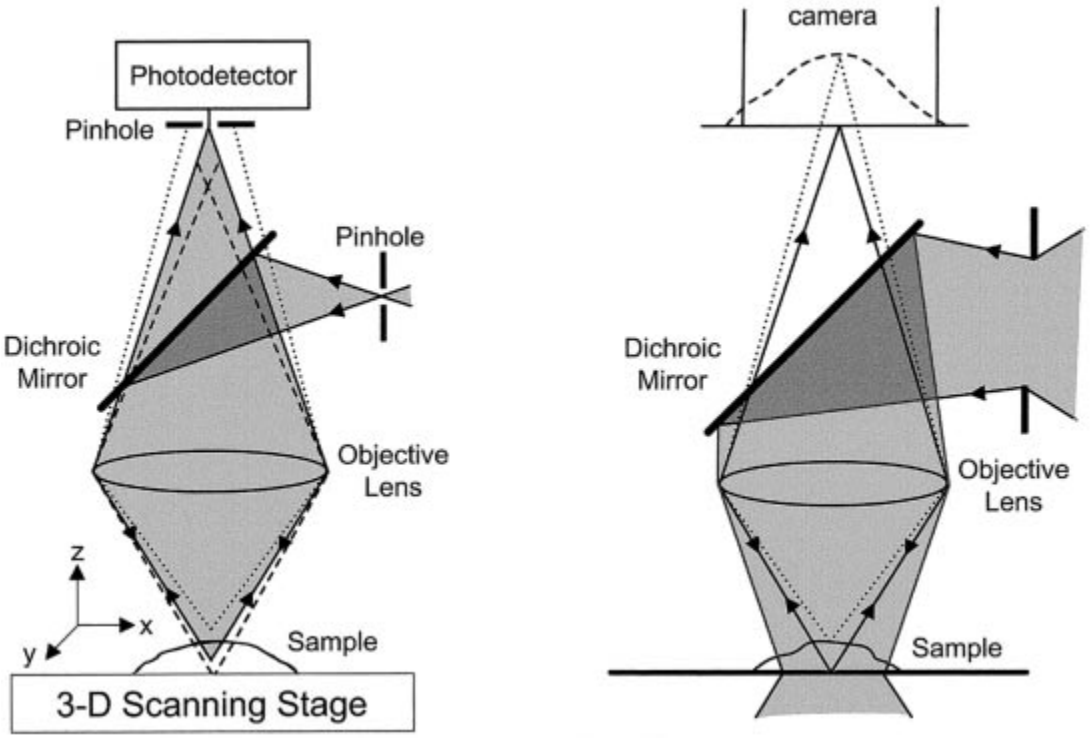

Figure 6. Difference between confocal (right) and conventional wide-field (left) microscopy. *Taken from (1).*

Emitting fluorophore is considered a point source of light. Point spread function (PSF) is used to describe the response of an imaging system to a point source of light or a point object. The light emitted by a fluorophore is diffracted at the objective lens of the microscope and thus forms a diffraction pattern known as Airy pattern. The center of this pattern (1st diffraction maximum) is known as Airy disk (**Figures 7, 8A,B**). (68) The point spread function of Airy pattern describes the intensity in radial space *PSF (r):*

$$PSF(r) = \left[\frac{2J_1(\rho)}{\rho}\right]^2$$

$$\rho = \frac{2\pi}{\lambda} rNA$$

$$NA = n \sin \alpha \ ,$$

(8,9,10)

where J_1 is Bessel function of the first kind of order one, λ is wavelength of the emitted light, r is a radial space coordinate, NA is the numerical aperture of the objective, n is refractive index of the enviroment near the objective lens and α is angular aperture of objective lens. (68)

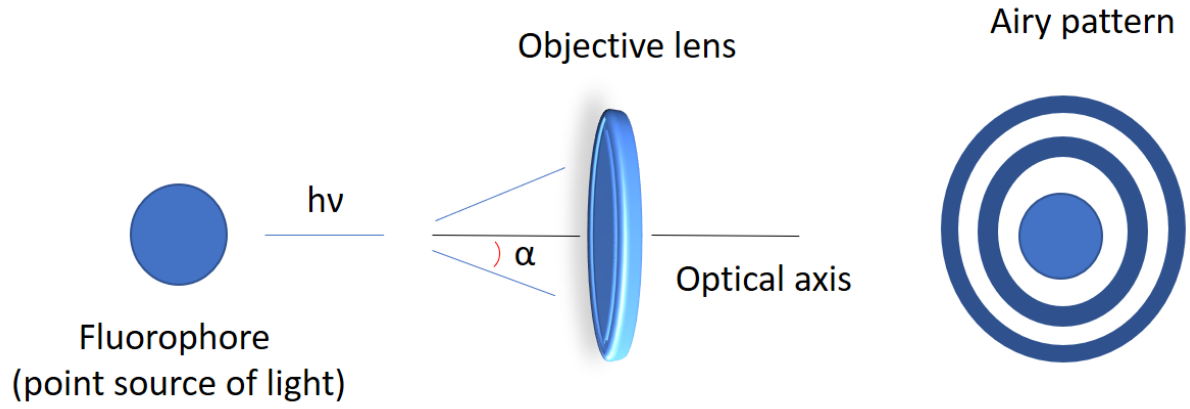

Figure 7. Schematic representation of how emitted light is diffracted by the objective lens in confocal fluorescence microscopy.

As mentioned above, the resolution in microscopy has a maximum that is given by the diffraction limit. The diffraction limit is described by the Rayleigh criterion which considers two images resolved if the Airy disc of the first image overlaps with the first diffraction minimum of the second image; this case is known as the Rayleigh limit (69). If the distance between the diffraction patterns of the two images is smaller than the Rayleigh limit the images are considered not resolvable (**Figure 8C,D**), if it is greater they are considered well resolved (**Figure 8E,F**). (68) The Airy pattern can be approximated as Gaussian function. Mathematically, the Rayleigh limit case corresponds to an intensity dip between the first diffraction maximums of two images of 26.4% for lateral resolution (perpendicular to optical axis – xy focal plane) in widefield microscopy:

$$\Delta r_{wf} = \frac{0.61\lambda}{NA}$$

(11)

In case of confocal microscopy, the diffraction happens both for excitation light and emitted light as both pass through objective lens. This means that:

$$\mathrm{PSF}_{confocal} = (\mathrm{PSF}_{lens})^2 \tag{12}$$

When applying the same principles as for wide-field microscopy on confocal microscopy we get a similar equation for lateral resolution:

$$\Delta \mathrm{r}_{confocal} = \frac{0.44\lambda}{NA} \tag{13}$$

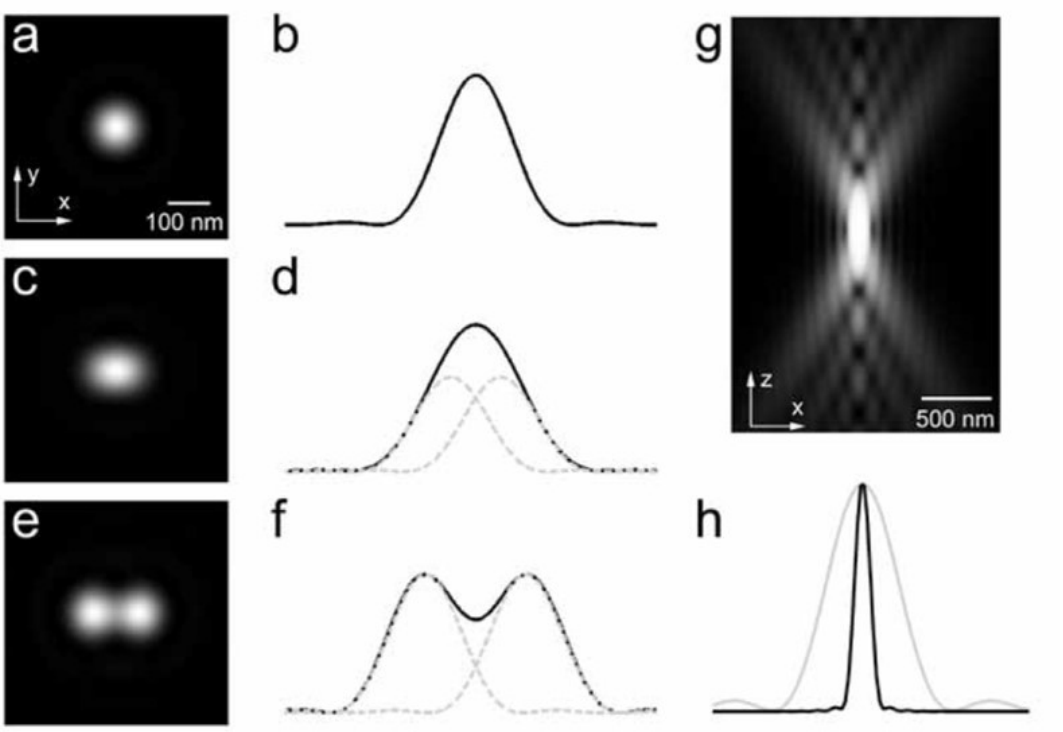

Figure 8. Diffraction limit in light microscopy. *λ = 500 nm and numerical aperture = 1.49 was used in these images.* ***A:*** *Point spread function (PSF) of a single point source.* ***B:*** *intensity cross-section of Airy disc from* ***A****.* ***C:*** *Image of two overlapping unresolvable point light sources.* ***D:*** *intensity cross-section of Airy discs from* ***C*** *along the x axis.* ***E:*** *Image of two resolvable point light sources.* ***F:*** *intensity cross-section of Airy discs from* ***E*** *along the x axis.* ***G:*** *Intensity map of the 3D PSF along the xz plane. The intensity is shown on log scale to emphasize the diffraction pattern. The central peak is much more elongated along the z axis.* ***H:*** *Comparison between the intensity cross-section along the focal axis z (black) and along the focal plane xy (grey). Taken from (70).*

In the case of axial resolution (along the optical axis – z axis) the situation is more complicated as it requires a consideration of 3D image with origin in the focus (**Figure 8G,H**). Point spread function for z axis is represented by equation:

$$PSF(z) = sinc^2 \frac{\zeta}{4} \left[\frac{sin \frac{\zeta}{4}}{\frac{\zeta}{4}} \right]^2$$

$$\zeta = \frac{2\pi}{n\lambda} zNA^2 ,$$

(14)

where z is an axial coordinate. By applying Rayleigh criterion on the axial PSF we get axial resolution for widefield microscopy:

$$\Delta z_{wf} = \frac{2n\lambda}{NA^2}$$

(15)

And a similar equation for confocal microscopy:

$$\Delta z_{confocal} = \frac{1.41n\lambda}{NA^2}$$

(16)

2.10. Fibroblast growth factor 2

Fibroblast growth factor 2 (FGF2), also known as basic fibroblast growth factor (bFGF), is a protein from the fibroblast growth factor family which plays many different roles in both physiological and pathological processes. Among the physiological processes where FGFs play important role are embryonic development, hematopoiesis, cell proliferation, cell differentiation and wound repair. (71) FGF2, specifically, is being investigated as a potential treatment component for various diseases and injuries, such as peripheral nerve injuries (72–74), with various tissue engineering applications being developed and undergoing clinical trials. (75–78)

On the other hand, FGF2 also plays a prominent role in many types of cancer as it promotes cell survival and angiogenesis. (79–83) This makes FGF2 also interesting as potential early marker of tumor growth or target for cancer therapy. (84) This should serve to illustrate the potential significance of research dedicated to this protein.

There are multiple FGF2 isoforms: 18 KDa low molecular weight isoform (LMW) and four high molecular weight isoforms (HMW) which contain additional aminoacids on the N-terminus. (85,86) These extensions serve as nuclear targeting signals for the transport into the nucleus. (87–89) The LMW isoform is localized mostly in cytosol, however, it can also be transported to the extracellular space, where it performs its autocrine cell survival signalling function. FGF2 lacks a signal peptide and has to be transported independently on ER/Golgi translocation system (90–92).

There are four types of unconventional protein secretion: (93) direct protein translocation across membrane (type I), ABC–transporter based secretion (type II) (94,95), vesicular pathways utilizing autophagy (type III) (96,97) and proteins that bypass Golgi complex to enter the plasma membrane (type IV) (98). There is strong evidence that FGF2 utilizes type I unconventional protein secretion pathway. (91,99)

Currently the unconventional mechanism of FGF2 secretion (**Figure 9**) is believed to occur in three steps: phosphatidylinositol-4,5-bisphosphate (PIP_2)–dependent binding of FGF2 to cellular membrane (I), formation of FGF2 oligomers which insert themselves into the membrane which results in membrane pore creation (II) and translocation of FGF2 across the membrane and return to monomeric state mediated by binding to heparan sulfate. (100,101)

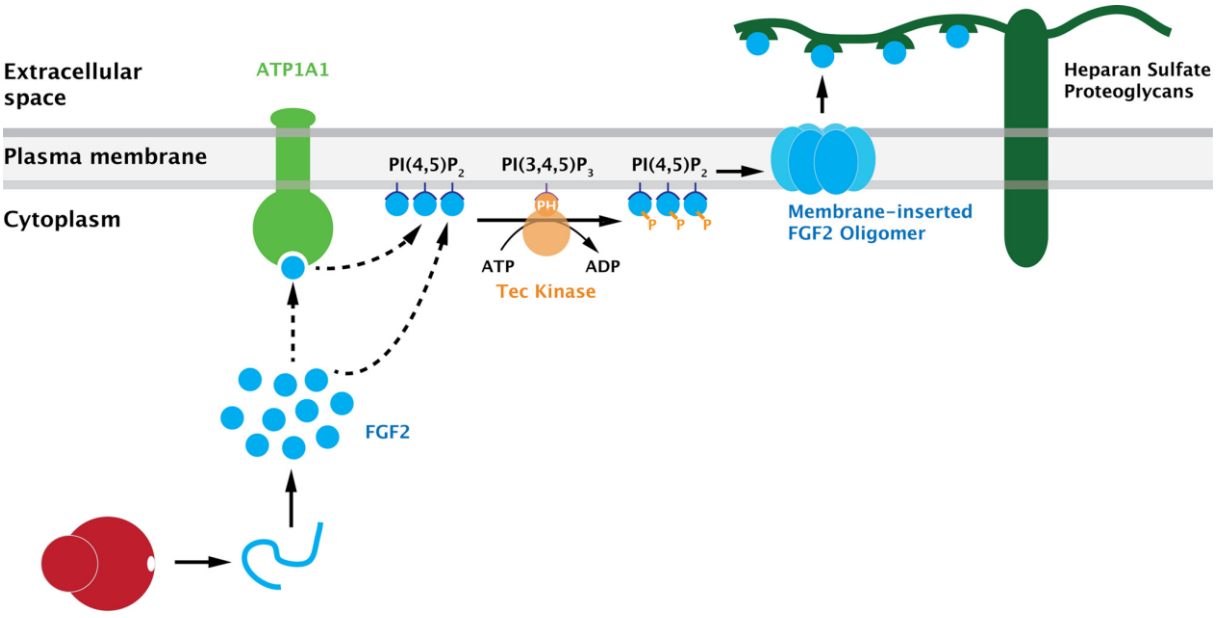

Figure 9. The unconventional mechanism of FGF2 secretion. From translation in ribosome to binding to heparan sulfate in the extracellular space. *Taken from (90).*

Many important factors have been identified in this process: In step I, binding to PIP_2 has been revealed to be mediated by basic residues of FGF2 (K128, R129 and K133) (102,103). Integral membrane protein Na/K ATPase, more specifically its α1-chain ATP1A1, also plays a role in FGF2 translocation mechanism, however, it remains unclear how exactly it is involved. (104) Phosphorylation of Y81 by Tec kinase improves membrane pore formation in step II by supporting insertion of FGF2 oligomers into the membrane (90,99,105). In regards to the oligomerization of FGF2, two important cysteine residues (C77 and C95) have been identified (106). When both of these residues are mutated, FGF2 can no longer form oligomers (103), which is detrimental to its ability to form pores. There is strong evidence suggesting that high oligomeric states (8 or 12) form pores that allow the translocation of FGF2 across the membrane. (99,103,106) Recently, dimers were suggested as intermediates for the formation of higher FGF2 oligomers based on TIRF microscopy experiments on live cells (107). Interaction of FGF2 with heparan sulfates is mediated by K133 residue. (103,108)

The individual role of both C77 and C95 in oligomer formation has been studied with the use of molecular dynamics simulations (**Figure 10**). Protein-protein contacts were studied for trimers where both C77-C77 and C95-C95 disulfide bridges are involved (103). Based on these results, it is suggested that C95-C95 disulfide bridge formation represents the first step in FGF2 oligomerization. It is further surmised that disulfide bridge formation occurs only once FGF2 is bound to the membrane because the reducing environment of the cytoplasm does not favour cysteine oxidation (106).

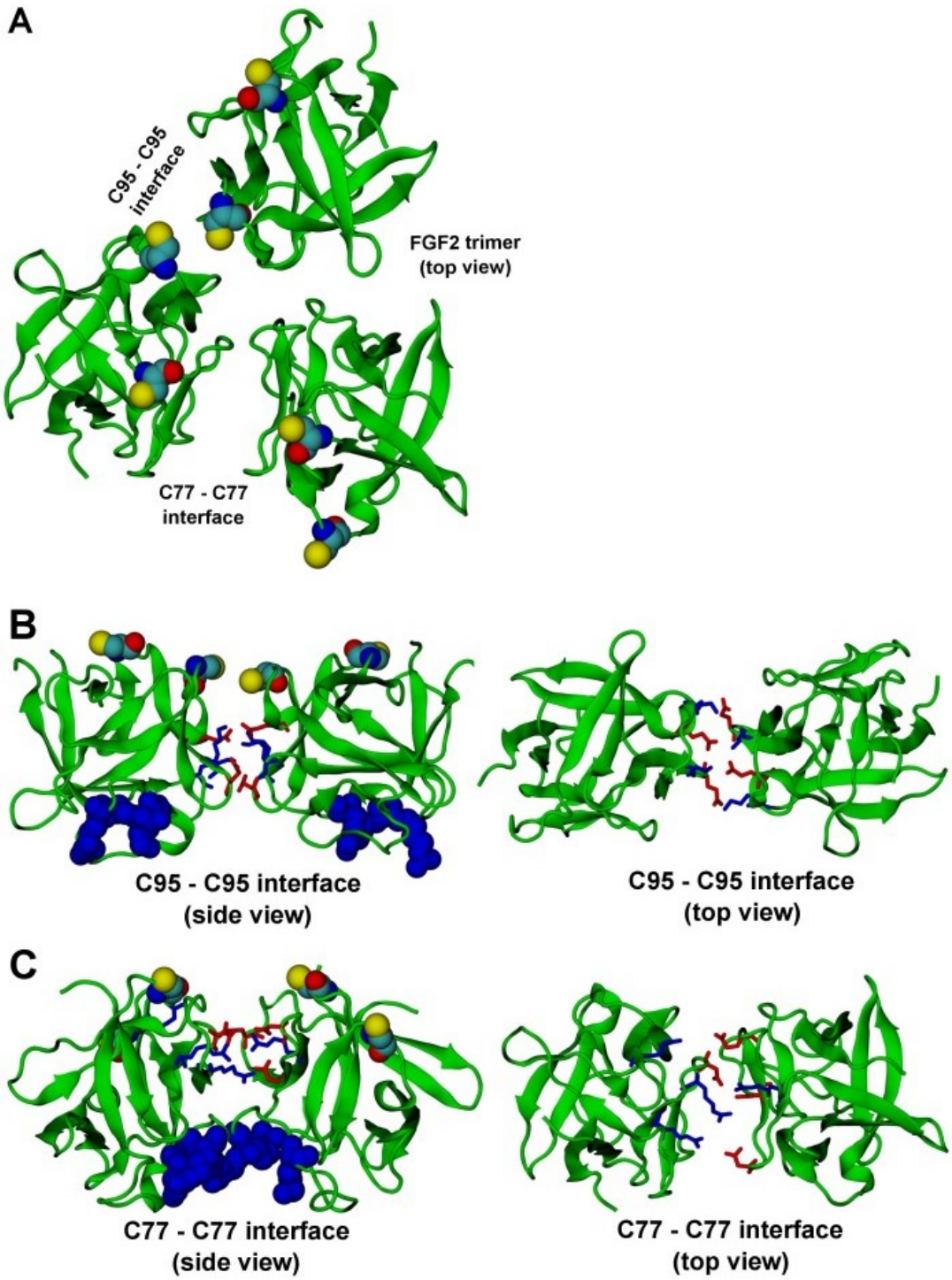

Figure 10. FGF2 trimer configurations. Snapshots representing the most populated structures in FGF2 trimer simulations. ***A****: Top view of the FGF2 trimer with C95 – C95 and C77 – C77 interfaces, where C95 and C77 are shown as colored van der Waals spheres (sulphur – yellow, oxygen – red, nitrogen – blue, carbon – teal). The trimer is split into two dimer interfaces shown in (B and C).* ***B****: The interface residues involved in C95–C95 disulfide-linked dimers.* ***C****: The interface residues involved in C77–C77 disulfide-linked dimers. The interface residues are depicted in stick representation, where negatively charged residues (D, E) are colored as red and positively charged residues (K, R) as blue. The PIP_2 binding pocket residues (K127, R128, K133) are rendered as blue van der Waals spheres. Taken from (103).*

3. Aims

The main aim of the thesis was to develop a simple and efficient fluorescence microscopy method that would enable studying formation of protein–induced membrane pores in real time. This would in turn make it possible to better understand the mechanisms that leads to opening of membrane pores and evaluate the lifetime of the pores.

The secondary and more specific aim was to use this approach and analyse the formation of the pores that are formed by fibroblast growth factor (FGF2) and its variants. More specifically, we wanted to study the effects of FGF2 cysteine mutations and Y81 phosphorylation on the ability of this protein to form membrane pores. While cysteines C77 and C95 have been suggested to play essential roles in FGF2 oligomerization (106), Y81 phosphorylation is supposed to stimulate membrane insertion of FGF2 oligomers (90,99,105). Our newly developed approach could thus provide useful insights into the first two phases of unconventional FGF2 translocation across the cellular membrane: binding of FGF2 to PI-(4,5)-P_2 on the membrane interface and PI-(4,5)-P_2 dependent oligomerization of FGF2 which is an important prerequisite for the formation of FGF2 pores. The method was designed to complement our ongoing oligomerization studies of FGF2 protein running at the department in collaboration with prof. Walter Nickel (Heidelberg).

4. Materials and methods

4.1. Chemicals

4.1.1. Lipids

L-α-phosphatidylcholine (PC) natural extract from bovine liver (Avanti lipids)

L-α-phosphatidylethanolamine (PE) natural extract from bovine liver (Avanti lipids)

L-α-phosphatidylserine (PS) natural extract from porcine brain, sodium salt (Avanti lipids)

L-α-phosphatidylinositol (PI)natural extract from bovine liver, sodium salt (Avanti lipids)

Sphingomyelin (SM) natural extract from chicken egg (Avanti lipids)

Cholesterol (Chol) natural extract from ovine wool (Avanti lipids)

1,2-dioleoyl-sn-glycero-3-phosphoethanolamine-N-(biotinyl), sodium salt (Avanti lipids)

L-α-phosphatidylinositol-4,5-bisphosphate (PIP_2) natural extract from porcine brain, ammonium salt (Avanti lipids)

Abberior Star 635P-labelled 1,2-dioleoyl-sn-glycero-3-phosphoethanolamine (DOPE) (λ_{ex} = 638 nm, λ_{em} = 651 nm, abberior)

The aforementioned lipids were mixed to form the lipid compositions that were used to prepare giant lipid vesicles (GUVs) by electroformation. (109) Membranes with 3 distinct compositions were prepared – plasma membrane like compositions (PM) with either 2 (PM2) or 5% (PM5) of PIP_2 and simplified phosphatidylcholine (PC) based composition which contained 10% PIP_2 (PC10) to facilitate efficient binding of FGF2. Exact lipid ratios can be found in **Table 3**.

Table 3. Lipid compositions that were used for the electroformation of GUVs. *PM2 stands for plasma membrane-like lipid composition containing 2% PIP_2 whereas PM5 stands for plasma membrane-like composition with 5% PIP_2 and PC10 for the membrane containing just phosphatidylcholine and 10% PIP_2.*

	PM2	**PM5**	**PC10**
Lipid	Molar percentage [mol%]		
PC	32	29	89
PE	10	10	
PS	5	5	
PI	5	5	
SM	15	15	
Chol	30	30	
DOPE-biotinyl	1	1	1
PIP2	2	5	10
DOPE-Abberior star	0.013	0.013	0.013

4.1.2. Fluorescent dyes

TRITC – dextran (Mw = 4094, Mn = 3803, λ_{ex} = 550 nm, λ_{em} = 571 nm, TdB Labs)

FITC – dextran (Mw = 4037, Mn = 2756, λ_{ex} = 493 nm, λ_{em} = 518 nm, TdB Labs)

Alexa fluor 532 (λ_{ex} = 532 nm, λ_{em} = 552 nm, Thermo Fisher Scientific)

Alexa fluor 647 (λ_{ex} = 649 nm, λ_{em} = 671 nm, Thermo Fisher Scientific)

4.1.3. Proteins

His-FGF2 (his tagged FGF2, wild type)

His-FGF2-GFP (his tagged FGF2 with fused GFP domain, λ_{ex} = 490 nm, λ_{em} = 509 nm)

His-FGF2-pCMF (his tagged FGF2 with phosphorylated Y81)

His-FGF2-C77A-pCMF (his tagged FGF2 with C77 mutated for A)

His-FGF2-C95A-pCMF (his tagged FGF2 with C95 mutated for A)

His-FGF2-C77A-C95A-pCMF (his tagged FGF2 with C77 mutated for A and C95 mutated for A)

FGF2 variants were provided and synthesized by prof. Walter Nickel and his group – Heidelberg University Center, Germany.

Biotin-BSA (Sigma)

Neutravidin (Thermo Fisher Scientific)

4.1.4. Other chemicals

HEPES (Sigma)

NaCl (Penta)

Sucrose (Sigma)

Chloroform (Sigma)

HEPES buffer (25 mM HEPES pH 7.4, 150 mM NaCl)

4.2. Other material/equipment

μ-Slide 8 well uncoated (ibidi)

pH meter (for buffer preparation)

Marcel OS3000 Osmometr

4.2.1. Electroformation

Velleman PC Function Generator PCGU1000

BK PRECISION 1550 power supply

Tektronix TDS 1002 oscilloscope

Heating block

Teflon chambers with platinum electrodes in the lid

Connecting cables

4.2.2. Microscope

The microscope setup is described in the section 'Imaging' (chapter 4.7).

4.3. Sample preparation

GUVs (giant unilamellar vesicles) were generated by electro-swelling using teflon chambers with platinum electrodes in the lid (110). Three different membrane compositions were used –

plasma membrane–like composition with either 2 or 5% of PIP_2 (PM2 and PM5) and phosphatidylcholine based composition which contained 10% PIP_2 (PC10). For visualization of the membrane 0.013 mol% Abberior Star 635P-labelled DOPE was added into all three compositions. For more details on these compositions see **Table 3**.

After receiving the lipids from Avanti, lipid mixes of each composition were made and these mixes were then dried and stored in small vials containing argon in a freezer. This was to prevent lipid degradation. For preparation of GUVs the dried lipid film was hydrated with chloroform to reach the final concentration of lipids of 1.5 mM. The chloroform solution was then added dropwise onto the Pt electrodes (3 µl per electrode) on which the chloroform evaporated. This way lipid film formed on the electrodes. Then 350 µl of a 300 mM sucrose solution (300 mOsmol/kg) was added into the teflon chambers for electroformation and a lid (with Pt electrodes) was used to close these chambers. Electroformation chambers were put into thermo block with constant temperature of 45°C. Electroformation was started 10 minutes after the chambers were put into thermo block for temperature equilibration. Velleman PC Function Generator PCGU1000 was used for function generation (GUV formation function: 10 Hz, 4 V pk-pk for 50 min; GUV detachment from electrodes function: 2Hz, 4 V pk-pk for 20 min) using Velleman PCLAB2000SE software, BK PRECISION 1550 power supply and Tektronix TDS 1002 oscilloscope (for control of the generated functions during electroformation).

After electroformation was finished, the sucrose solution containing GUVs was put into 2 ml Eppendorf tubes and 1.15 ml of HEPES buffer was added (305 mOsmol/kg). Eppendorf tubes were then centrifugated (1200x g; 25°C; 5 min). GUV pellet was resuspended in a small volume of buffer and put into 15 ml plastic tubes where it was diluted again in 12 ml of HEPES buffer. This was followed by a second centrifugation (1200x g; 25°C; 5 min). The point of this procedure was to exchange sucrose for buffer (closer to natural environment for FGF2 which is added later) on the outside of GUVs and to remove small vesicles and lipid waste. The supernatant was removed and the GUV pellet was resuspended in 350 µl of HEPES buffer. Imaging chambers (Ibidi) were incubated with 0.1 mg/ml Biotin-BSA solution for 20 minutes. After the incubation, the chambers were washed 3 times with MiliQ water. Then the chambers were incubated with 0.1 mg/ml Neutravidin solution. After the incubation, the chambers were washed 3 times with HEPES buffer. Then 175 µl of GUVs in buffer were added into the chamber along with a FGF2 variant in HEPES buffer (to reach either 100 or 200 nM final concentration of FGF2 in the chamber) and extra HEPES buffer to reach a total of 350 µl.

GUVs were immobilized in the imaging chamber via biotinylated PE binding to neutravidin which was also bound to biotin-BSA that was adsorbed to the imaging chamber surface. Immobilization of GUVs is necessary for successful tracking of individual GUVs during double leakage single GUV assay.

Osmolarity of sucrose and HEPES buffer was determined by using a Marcel OS3000 Osmometr. Osmolarity is important for stability for GUVs. The goal is to have the same osmolarity on the inside of the GUV and on the outside so that the osmotic pressure difference is close to 0. Because part of the sucrose solution evaporates during electroformation (thus increasing the osmolarity) osmolarity of sucrose solution is lower than that of HEPES buffer to serve as a compensation.

4.4. Searching for the 'optimal' membrane composition – single leakage assay

Membrane composition is extremely important when studying proteins that bind to membranes and function on or in the membrane. To figure out the 'optimal' membrane composition for FGF2 experiments, several single leakage assay experiments were conducted. The 'optimal' membrane should have a composition as close to the composition of cellular membranes as possible, have low unspecific leakage (i.e. the membrane should be intact with no defects) and allow for efficient binding of FGF2 to the membrane surface.

GUVs were incubated for 3 hours with FGF2-GFP at either 100 nM or 200 nM final concentration. Some of these experiments were done with a use of a heating chamber H301-mini (Okolab), heating the sample to 37°C for the first 30 minutes of the incubation with FGF2, or in some cases for the whole incubation. After 2,5 hours of incubation, a small fluorescent dye was added (1 µl of 70 µM Alexa fluor 532 solution). At the end of the incubation, a part of the imaging chamber was scanned using a confocal fluorescence microscope.

4.5. Principle of double leakage single GUV assay (DLSGA)

As mentioned in the Aims section, the main goal of the thesis is to develop a simple and efficient fluorescence microscopy method that would enable studying formation of protein-induced membrane pores in real time. The method should serve to elucidate intricacies of the mechanism of protein pore-formation.

In order to achieve this, a new approach was developed: tracking large number of GUVs in the presence of pore-forming proteins in the course of time. To determine if and when the pores

were open, if or when they closed, two different leakage dyes differing in the emission wavelength have been added sequentially into the solution surrounding the GUVs. The GUVs were measured in multiple steps, and after each measurement, a fluorescent dye was either added or removed from the solution. The experiment was conducted in such a way that the identity of each GUV was known in the course of the entire experiment. This allowed us to divide all imaged GUVs into 6 distinct categories, depending on the leakage behaviour of each GUV. In this way we could discover differences in the formation of FGF2 pores by single/double cysteine mutants of FGF2 (more details can be found in chapter 4.8).

4.6. Development of double leakage single GUV assay

The double leakage assay experiment was done for six FGF2 variants using PM + 2% PIP_2 membranes incubated with 200 nM FGF2: Wild type, pCMF, FGF2-GFP, C77A C95A pCMF, C95A pCMF and C77A pCMF. Two sets of fluorescent leakage dyes differing in size were used for the experiments – small dyes: Alexa fluor 532, Alexa fluor 647 – and 4 KDa dextran dyes: TRITC-dextran and FITC-dextran.

The assay consists of 4 different steps: 1) incubation of GUVs with FGF2 protein; 2) addition of the first fluorescent dye followed by Measurement I; 3) washing out excess protein and the first dye followed by Measurement II and 4) addition of the second fluorescent dye followed by Measurement III (see **Figure 11** for a detailed scheme explaining the timeline of the experiment).

More specifically, the entire incubation time was 3 hour long (before Measurement I). First, the sample was heated in the H301-mini (Okolab) heating chamber for 30 minutes, during this time FGF2 was already present. After 2.5 hours of incubation, the first fluorescent dye was added (either 1 µl of 70 µM Alexa fluor 532 solution or 3.5 µl of 100 µM TRITC-dextran). At the end of the incubation, a part of the imaging chamber was scanned using a confocal fluorescence microscope (Measurement I). The xy positions of the individual vesicles were saved so that they could be returned to later in Measurement II and Measurement III. Then the dye and the protein were washed out from the imaging chamber in multiple steps by adding HEPES buffer until no signal from the dye was visible on the outside of GUVs. This was done carefully so that GUVs stayed immobilized via biotin-neutravidin interaction. 30 minutes after the end of this procedure, the same part of the imaging chamber was scanned again (Measurement II). Afterwards, the second fluorescent dye was added into the imaging chamber (either 2 µl of 70 µM Alexa fluor 647 solution or 3.5 µl of 100 µM FITC-dextran solution in case of dextran

double leakage experiments). 30 minutes after adding the dye, the same part of the imaging chamber was scanned for the third time (Measurement III).

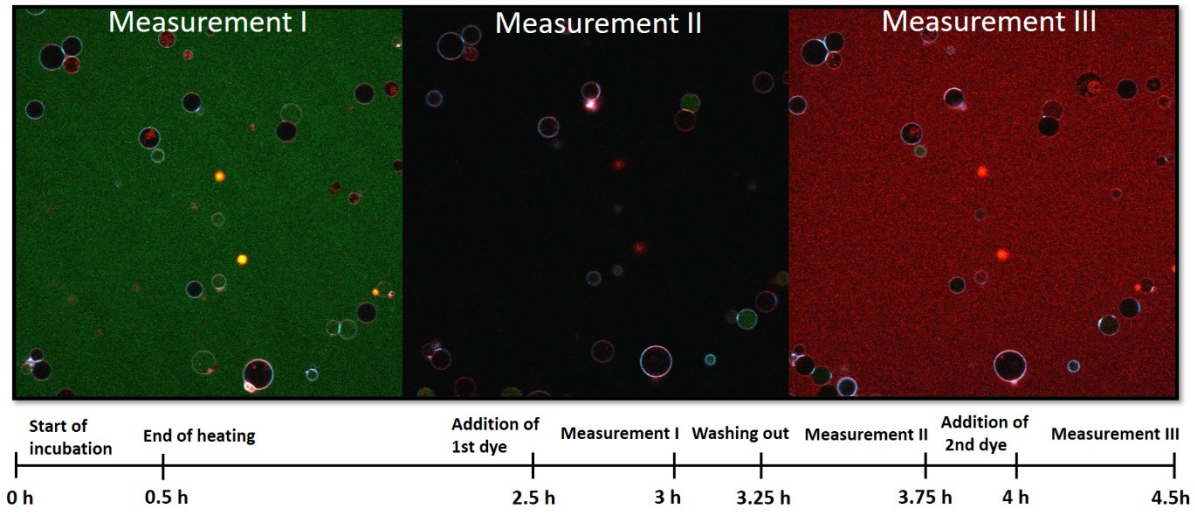

Figure 11. The series of images recorded when performing the double leakage single GUV experiment with small dyes and FGF2-GFP protein; the timeline of the experiment is shown under the images. ***Measurement I*** *is done after 30 minutes of incubation with the first fluorescent dye, in this case Alexa fluor 532.* ***Measurement II*** *is done 30 minutes after the first fluorescent dye and the excess of the protein were washed out from the solution.* ***Measurement III*** *is done after 30 minutes of incubation with the second fluorescent dye, in this case Alexa fluor 647. The same area of the imaging chamber has been measured throughout the experiment, which allows for tracking the leakage states on the same GUV in each step. This is only possible because of immobiliazation of GUVs via biotynyl-neutravidin interaction as described above.*

4.7. Imaging

The confocal microscope setup consists of a modified commercial Olympus FluoView 1000 system. To image individual GUVs for their leakage state, three colour (B/G/R) imaging FluoView software utilizing built-in photomultiplier tubes (PMT), beam-splitters and band-pass or long-pass filters selected from built-in wheels was used. The excitation system is home-built and consists of LDH-D-C-470, LDH-D-C640 diode laser heads (driven by PDL 828 Sepia II – PicoQuant, Berlin, Germany) and 543 nm HeNe continuum wave laser. The output of the three laser heads is coupled to a single optical fiber. After entering the microscope, the beam passes through a pinhole aperture and is then brought onto a triple-band 488/543/633 excitation dichroic mirror. The beam then goes through the water immersion objective (UPlanSApo 60x w, NA 1.2) and then into the sample (imaging chamber). The fluorescence signal is collected by the same objective, passes through 100 µm wide pinhole and is divided between

three photomultiplier tubes by dichroic mirrors. The first dichroic mirror transmits all light with wavelength longer than 560 nm and reflects all the remaining light into the first PMT (blue channel, 525 V) with the band-pass filter 490 – 525 nm. The transmitted light comes in contact with the second dichroic mirror which transmits light with wavelength longer than 640 nm and reflects the rest of the light onto the second PMT (green channel, 735 V) with band-pass filter 560 - 620 nm. The transmitted light then comes into the third PMT (red channel, 835 V) with the long-pass filter 650+ nm.

For dextran experiments the voltage in the first PMT was 735 V, same as the second PMT (in dextran experiments emission from leakage dyes was detected by these two PMTs and having equal voltage was preferable). In case of small dye experiments the voltage 525 V for blue channel was used for better contrast when looking at FGF2-GFP binding to GUVs.

For measurements a part of the imaging chamber was scanned. Each image was 512 x 512 pixels, a total of 211.5 x 211.5 µm per image. Fluorescence intensity was collected for 8 µs per pixel. Intensities for each channel were measured for each pixel. Measurements were done at 25°C. For details about all the used dyes and fluorescently labelled molecules see **Table 4**.

Table 4. Used fluorescent dyes or their analogues with their excitation and emission wavelengths combined with the information about the excitation laser for each dye and their main detection channel.

Used fluorescent dyes / labelled molecules	Excitation wavelength [nm]	Emission wavelength [nm]	Excitation laser wavelength [nm]	Detection channel
His-FGF2-GFP	490	509	470	Blue, Green
Abberior star 635P-DOPE	638	651	640	Red
Alexa fluor 532	532	552	543	Green
Alexa fluor 647	649	671	640	Red
TRITC-dextran	550	571	543	Green
FITC-dextran	493	518	470	Blue

4.8. Analysis

Analysis was done by reviewing the recorded images in Image J (software) and determining the intensity of fluorescence for each channel separately in the interior and exterior of GUVs.

GUVs were divided into three groups based on their leakage: all or none leakage (the intensity of fluorescence on the outside and inside of a GUV is the same), graded leakage (the intensity of fluorescence that corresponds to the dye on the inside is lower than on the outside) and no leakage.

For the double leakage single GUV assay, GUVs were divided into six groups (A-F) based on their state during each of the three scans (**Figure 12**). Minimum of 100 GUVs were analysed for each experiment while having at least 50 leaky GUVs.

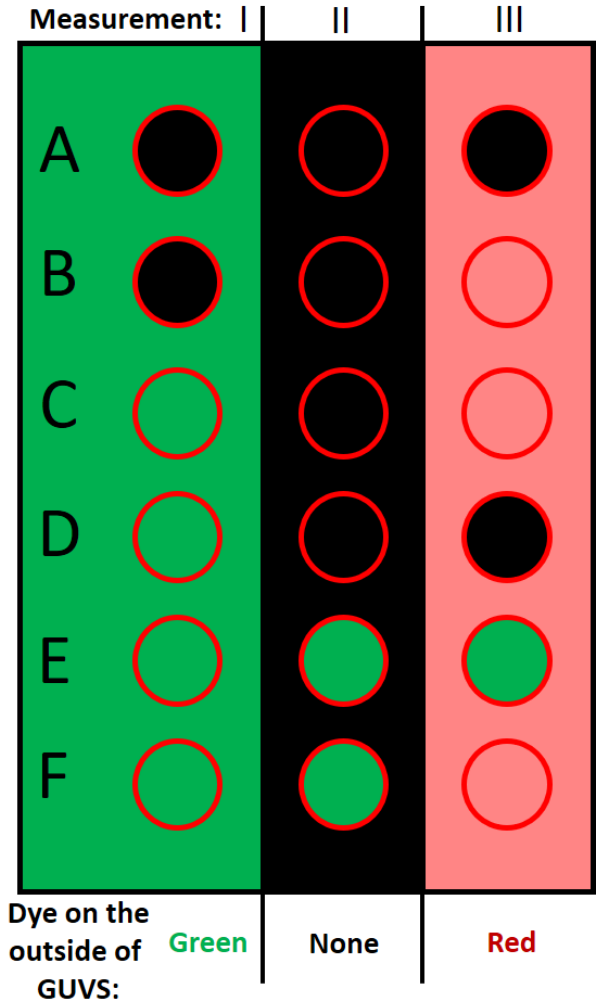

Figure 12. GUVs divided into the following groups (A-F) based on their state in the double leakage single GUV assay. *The red circles represent the GUVs, green on the inside and on the outside of the GUVs depicts fluorescent dye Alexa fluor 532 used in the assay. Black on the inside and on the outside of the GUVs means that no dye was present. Red on the inside and on the outside of the GUVs depicts fluorescent dye Alexa fluor 647 that was used in the assay.* ***A:*** *GUVs that were intact in the course of the entire experiment.* ***B****: GUVs that became leaky after free FGF2 and the first fluorescent dye were removed from the solution.* ***C:*** *GUVs that were leaky in the course of the entire measurement.* ***D:*** *GUVs that were leaky when the first fluorescent dye was present and shortly after it was removed, but not after the second dye was added* ***E:*** *GUVs that were leaky when the first fluorescent dye was present; pores closed before the first fluorescent dye was removed.* ***F:*** *GUVs that were leaky when the first fluorescent dye was present; pores closed before the first fluorescent dye was removed but reopened after the second fluorescent dye was added.*

5. Results and discussion

5.1. Choosing optimal membrane

The membrane of a GUV may become permeabilized naturally (by lipid defects) even without the presence of pore-forming proteins. This is a problem because there is no way to distinguish between defects of the membrane and protein-mediated leakage. For more accurate results it is highly desirable to eliminate this effect. It can theoretically be achieved by using a membrane composition that is not prone to defects, however this is rather problematic, because in nature cellular membranes are a lot more complicated than just a combination of various lipids.

We had three objectives when choosing the optimal membrane composition: minimizing unspecific leakage, being as close to the composition of the cellular membrane as possible and facilitating sufficient binding of the protein. In total, we tested three membrane compositions using the single dye leakage assay introduced in chapter 4.4: PC + 10% PIP_2, PM + 2% PIP_2 and PM + 5% PIP_2. Both PC10 and PM5 compositions have shown decent binding (**Figure 13**) of the protein to the membrane. This resulted in increased fraction of leaky GUVs (FGF2 causes leakage of GUVs by insertion of its oligomers into the membrane). Unfortunately, these compositions also had a relatively high leakage of the blank (around 20% GUVs were leaky even without the protein in the sample). On the other hand, PM2 composition exhibited a relatively low leakage of the blank (12%). However, it also had a very weak binding of the protein at a relatively high protein concentration used (100 nM). This was mitigated by doubling the concentration of protein (**Table 5**). Both types of leakage mechanisms were observed: graded leakage (slow rate of diffusion through membrane, concentration of dye does not equilibrate across membrane) (111–113) and all or none leakage (pores have sufficient size and stability to allow for concentration of dye on the outside of the GUV to equilibrate with inside of the GUV) (111,112,114–117).

Table 5. Results and conditions of single dye leakage assay experiments that were done to determine the optimal membrane composition. *Because graded leakage was very low a row is included with information about total leakage instead (percentage of GUVs with all or none leakage + percentage of GUVs with graded leakage).*

Membrane composition	**PC + 10% PIP2**		**PM + 5% PIP2**		**PM + 2% PIP2**			
Presence of protein	blank	FGF2-GFP	blank	FGF2-GFP	blank	FGF2-GFP		
Concentration of protein and temperature	0 nM, RT	100 nM, RT	0 nM, RT	100 nM, RT	0 nM, RT	100 nM, RT	200 nM, RT	200 nM, heating
Percentage of GUVs with all or none leakage	22%	41%	18%	41%	12%	20%	41%	55%
Percentage of GUVs with all or none or graded leakage	23%	42%	20%	45%	12%	21%	41%	55%

Based on these results, we decided to further optimise experimental conditions for the PM2 membrane, as it had the least leaky blank and represents biological membranes in the best way. To further improve the amount of membrane-bound protein, experiments with 300 nM concentration of FGF2-GFP were conducted. However, this high concentration had detrimental effects on the stability of GUVs, which led to their bursting. Another approach to increase the binding of FGF2-GFP to GUVs was heating the sample to 37°C – the temperature at which the human protein normally operates *in vivo*. Experiments revealed that 37°C visibly improves binding of FGF2-GFP to the membrane in the first few minutes after addition of the protein. Heating the sample for the whole experiment led to the decrease in the stability of the membrane and higher leakage of the blank. Therefore, the optimal approach was determined to be: heating the sample only at the beginning and then letting it cool down to 25°C for the rest of the experiment. In this way, protein binding was improved without decreasing the stability of the membrane.

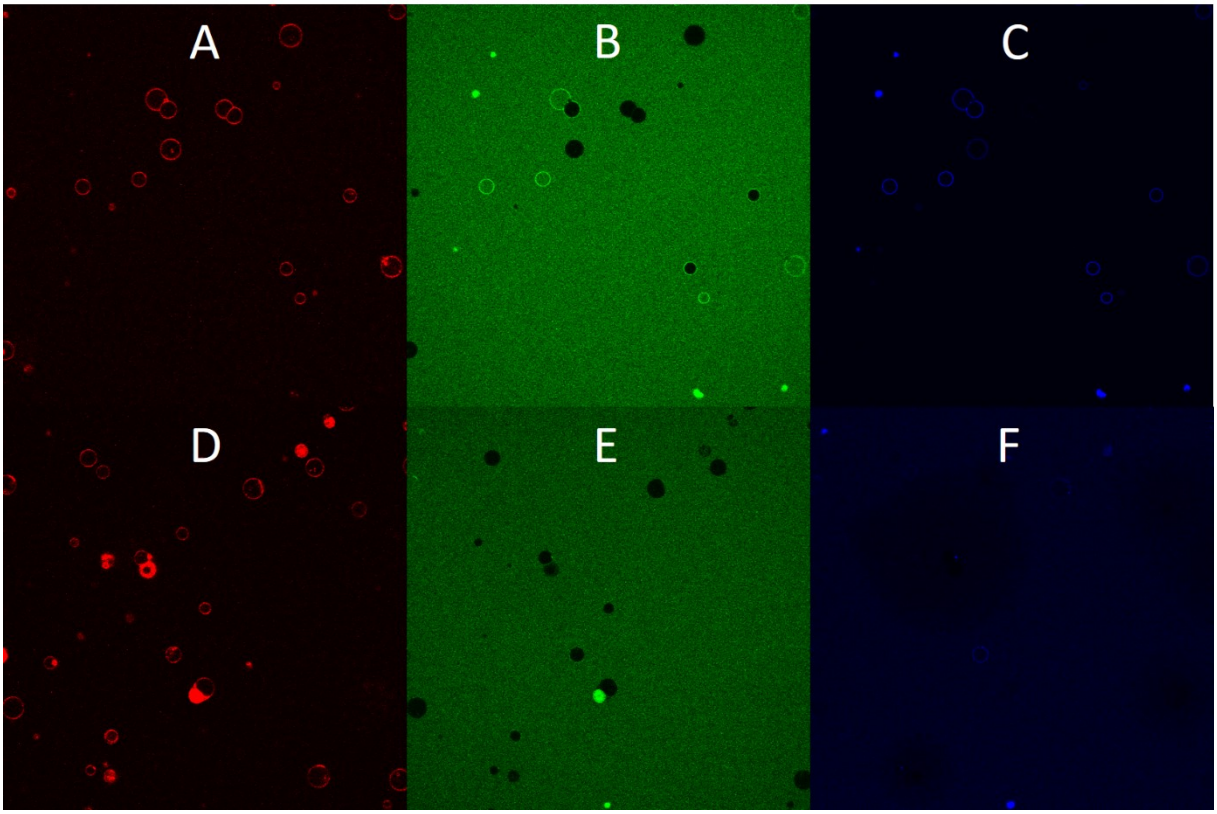

Figure 13. Examples of his-FGF2-GFP binding to PIP_2 on GUVs. A-C *Shows the same image but each time displayed using photon-counts from a different channel. The same holds true for* ***D-F. A,D****: Abberior star 635p labelled DOPE is detected in the red channel – this shows the membrane of GUVs as well as some random lipid aggregates.* ***B,E****: Alexa fluor 532 is detected in the green channel which shows whether the GUVs are leaky or not (the dye is present in the outside of the GUVs but only some GUVs contain the dye in the GUV interior).* ***B:*** *It is also possible to see GFP fluorescence on the membrane in the green channel which indicates sufficient binding of FGF2-GFP fusion protein..* ***C,F****: blue channel detects only fluorescence from GFP.* ***C:*** *fluorescence in blue channel confirms that most GUVs have significant amount of FGF2 bound to their membrane.* ***F:*** *insufficient binding – GFP fluorescence is not visible on most GUVs despite the fact that the protein can be seen in the bulk. Binding of FGF2 to GUVs is very uneven – some GUVs seem to have no FGF2 in their membrane or an amount below the detection limit while other GUVs have high amounts of FGF2-GFP as indicated by the high intesity in the green and blue channel (from GFP fused to FGF2).*

5.2. Double leakage single GUV assay

Having determined suitable experimental conditions and membrane composition to study FGF2-mediated permeabilization, the task was to develop a method that would provide details about the formation of FGF2 pores, being a prerequisite for the translocation of FGF2 across the membrane. A method introduced in the paper by Fuertes et al (118) was used as a starting point for the development. In this paper, the authors used GUVs as a model for the mitochondrial membrane to study pores formed by protein Bax α5. In the experiment, GUVs were added to an observation chamber containing the solution of Bax α5 and a fluorescent dye.

The GUVs were observed for the next two hours during which the dye permeated some of the GUVs. Afterwards, second fluorescent dye was added and 15 minutes after that a third fluorescent dye. The experiment was done to study the pore size in the course of time. This method, however, does not account for unspecific leakage. Therefore, it cannot discriminate between permeabilization caused by random defects of the membrane and actual opening of protein-induced membrane pores. It is also not suitable to study different variants of the same protein as it only focuses on the kinetics of leakage.

We re-designed the assay to be more specific towards different mechanisms of membrane permeabilization (to account for unspecific leakage). Instead of focusing on the kinetics, we decided to track individual GUVs in the course of time and to focus on the mechanism of the leakage by observing a large number of single GUVs in time (more details in chapters 4.5 and 4.6). Importantly, with this method in our hands, we can track one and the same GUV over three phases of the experiment (Measurements I-III), which allows us to get more specific information about the formation and stability of the pores. In addition to that, we can get this information for up to 300 GUVs in a single experiment and consistently for at least 150 GUVs in a single experiment. This large ensemble approach allows the differences between the variants of same the protein to become noticeable.

Before discussing the results of the double leakage single GUV assay it may be useful to show the impact of the various cysteine mutations on the oligomerisation behaviour of FGF2. These measurements were done by Petra Riegrová PhD. and Sabína Macharová PhD. at the Department of Biophysical Chemistry, J. Heyrovsky Institute of Physical Chemistry of the Czech Academy of Sciences. The results were obtained by dual-color FCS measurements (103,119) using PM2 membrane composition. Both leaky and non-leaky GUVs were measured. FGF2 causes leakage of GUVs by formation of oligomers that insert themselves into the membrane. (103,106) By measuring both leaky and intact GUVs they were able to get some inclination about oligomeric size required for pore formation. Measurements that were done on intact GUVs show that not all FGF2 oligomers can form pores (not all oligomers are capable of membrane insertion). By comparing the brightness of a monomer to the brightness of oligomers, they were able to determine the average aggregation number for FGF2 variants on both permeabilized and intact GUVs (**Figure 14**). It is known that the C77A C95A variant is practically incapable of forming oligomers and has been shown to be also incapable of translocation across cellular membrane (106). This variant was used to determine the brightness of a monomer unit in these measurements. C95A variant forms almost exclusively only dimers.

In contrast, C77A variant can form larger oligomers with median oligomeric size of 6 for leaky GUVs and 7 for intact GUVs. Wild type variant is slightly different as it has median oligomeric size of 7 for leaky GUVs and 5 for intact GUVs. It should be noted that there is no way to determine with certainty whether GUVs leaked because of FGF2 pore-formation or random membrane defects. It is however safe to assume that most of the measured leaky GUVs were leaky because of FGF2 as it was detected in the membrane and FGF2 does significantly increase leakage (**Table 5**) as compared to the blank.

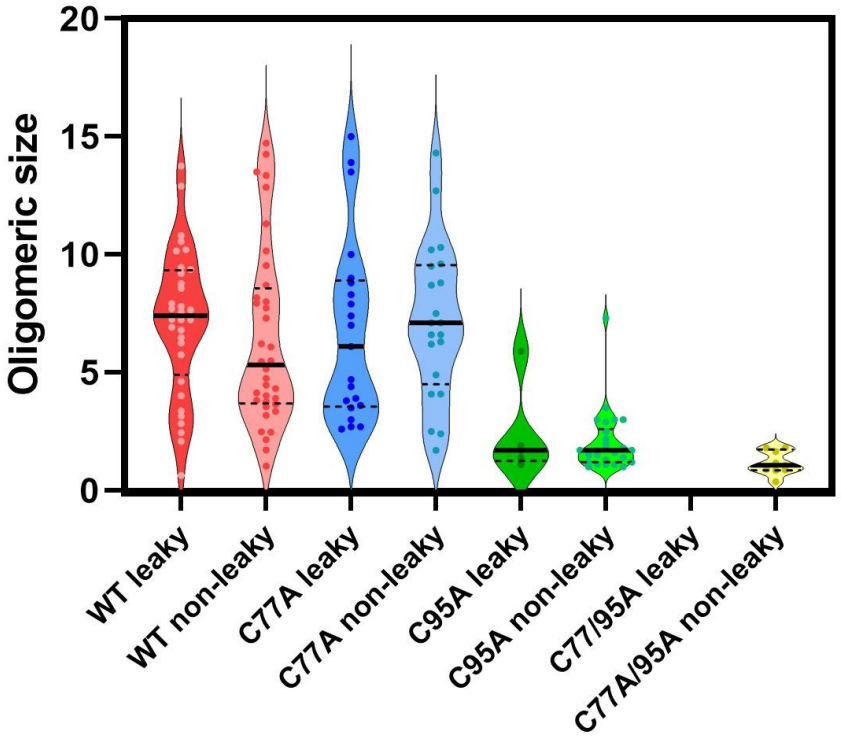

Figure 14. Functional correlation of oligomeric size with membrane pore formation for four FGF2 variants. *Median values shown as thick black lines and 95% confidence intervals are indicated by dashed black lines. The results for single cysteine mutants have not yet been published at the time when this thesis was written.*

The double leakage single GUV assay experiments were done for six variants of FGF2 with GUVs having the 'optimal' membrane composition as determined in the previous step. Results of Measurements I, II and III for each variant can be found in **Table 6**. By comparing these results with the results obtained for the blank (**Table 5**), it is evident that all variants of FGF2 permeabilize the membrane. The Measurement I of the double leakage single GUV assay is actually the single GUV assay introduced in chapter 4.4 – the methods only start to differ after this step. The results are perfectly comparable.

Even the C77A C95A pCMF variant which almost never oligomerizes due to its mutations (103) (pores are believed to be formed by FGF2 oligomers) exhibits some degree of leakage (**Table 6**). This is likely caused by adsorption of the protein to the membrane surface which can destabilize the membrane (120). For this reason, experiments with double cysteine mutant were considered as the blank to eliminate effects of unspecific leakage in further analysis (**Figures 15C, 16C**). Variant C77A pCMF which has only one cysteine mutated did cause significant leakage (86% GUVs were permeabilized), which suggest that it retains the ability to form oligomers that are inserted into the membrane. This is in agreement with the results shown in **Figure 14**. Surprisingly, the same can be said about the other single cysteine mutant C95A pCMF, which according to the results shown in **Figure 14** forms almost exclusively only dimers. This is an interesting result because only higher oligomeric states were suggested to be responsible for translocation (99,106,120). However, in recent experiments that were done on cells where translocation of FGF2 across the cellular membrane was observed, the researchers were only able to detect low oligomeric states with dimers being by far the most prevalent (107). They speculated, based on the previous results, that this could be caused by the fact that higher oligomeric states of FGF2 are highly dynamic and transient. This would explain why they were not able to detect these higher oligomeric states in the experiment. Therefore, they proposed that the dimers are important intermediates, as was predicted earlier by molecular dynamics simulations (120). Our results for C95A variant on the other hand strongly suggest that dimers are capable of pore-formation and thus protein insertion. In conjunction with the aforementioned experiments on cells, it seems that dimers might be the main biological oligomeric state that is responsible for the unconventional mechanism of FGF2 secretion. This also brings into question the biological relevance of C95 as its replacement by alanin does not prevent formation of stable pores.

In general, the FGF2 variants with phosphorylated Y81 (pCMF) exhibit higher leakage in Measurement I than variants without phosphorylation. This is due to significantly higher percentage of graded leakage. Phosphorylation of Y81 has been shown to stimulate membrane insertion of FGF2 oligomers (90,99,105). Wild type and FGF2-GFP variants show significant increase in leakage (20% increase) in Measurement III (later in the experiment, after the protein has been removed from the solution). This suggests that without phosphorylated Y81 it takes longer time for FGF2 oligomers to undergo insertion into the membrane and pore-formation, however, it is still achievable to a similar degree given enough time.

Table 6. Double leakage single GUV assay results for six variants of FGF2 using PM2 membrane composition. *Fractions of leaky GUVs containing small fluorescent dyes – Alexa fluor 532 and Alexa fluor 647. Both types of leakage were observed. Total leakage represents sum of percentages for both types of leakage.*

FGF2 variant	Wild type	PCMF	FGF2-GFP	C77A PCMF	C95A PCMF	C77A C95A PCMF
Types of leakage	**All or none; graded; total**					
Percentage of GUVs containing Alexa Fluor 532, measurement I	50%; 12%; 62%	44%; 43%; 87%	52%; 17%; 69%	54%; 32%; 86%	48%; 25%; 73%	29%; 9%; 38%
Percentage of GUVs containing Alexa Fluor 532, measurement II	2%; 12%; 14%	5%; 38%; 43%	2%; 8%; 10%	18%; 32%; 50%	1%; 21%; 22%	1%; 4%; 5%
Percentage of GUVs containing Alexa Fluor 532, measurement III	1%; 11%; 12%	1%; 35%; 36%	2%; 5%; 7%	16%; 31%; 47%	0%; 6%; 6%	0%; 3%; 3%
Percentage of GUVs containing Alexa Fluor 647, measurement III	67%; 3%; 70%	36%; 14%; 50%	68%; 16%; 84%	22%; 9%; 31%	49%; 27%; 76%	29%; 7%; 36%
Percentage of GUVs containing either green or red dye, measurement III	68%; 14%; 82%	37%; 49%; 86%	70%; 21%; 91%	38%; 40%; 78%	49%; 33%; 82%	29%; 10%; 39%

Because we track individual vesicles in the course of time, it is possible to divide them into groups based on pore opening dynamics and stability (**Figure 15,16**). Detailed description of each group can be found in chapter 4.8 (**Figure 12**). At least 100 total GUVs were measured and analysed for each FGF2 variant containing at least 50 leaky GUVs (groups B-F).

Here, it should be noted that out of the three phases of the unconventional translocation mechanism of FGF2 we have been only able to observe phase one – binding of FGF2 to the membrane and phase two – oligomerization and insertion of FGF2 oligomers resulting in pore formation. As for phase three – the translocation of FGF2 oligomers across the cellular membrane could not be observed. *In vivo,* this process is extremely fast, it only takes 200 ms on average from FGF2 binding to the membrane to its translocation (107). In this experiment, the protein is present on the membrane for 4.5 hours and binding is visible within the first few minutes so the fact that translocation is not observed is definitely not because of lack of time.

This is probably caused by the fact that some of the components that take part in the unconventional translocation mechanism of FGF2 are missing from our experiments. This means that the translocation was either altogether impossible or it happened in such a small degree to be indistinguishable from noise. If translocation occurred we should observe increase in intensity in the blue channel from FGF2-GFP on the inside of GUVs.

A significant amount of GUVs with reconstituted double cysteine mutant does not become leaky when the dye is present in the bulk – scenario A (47% of all GUVs, **Figure 15B**). This is expected as this variant almost never forms oligomers that could then be inserted into the membrane and cannot thus cause the leakage during this event. As mentioned above, experiments with this variant were considered as experiments with the blank. After subtracting the blank from the data for the other variants, the results become clearer (**Figure 15C**).

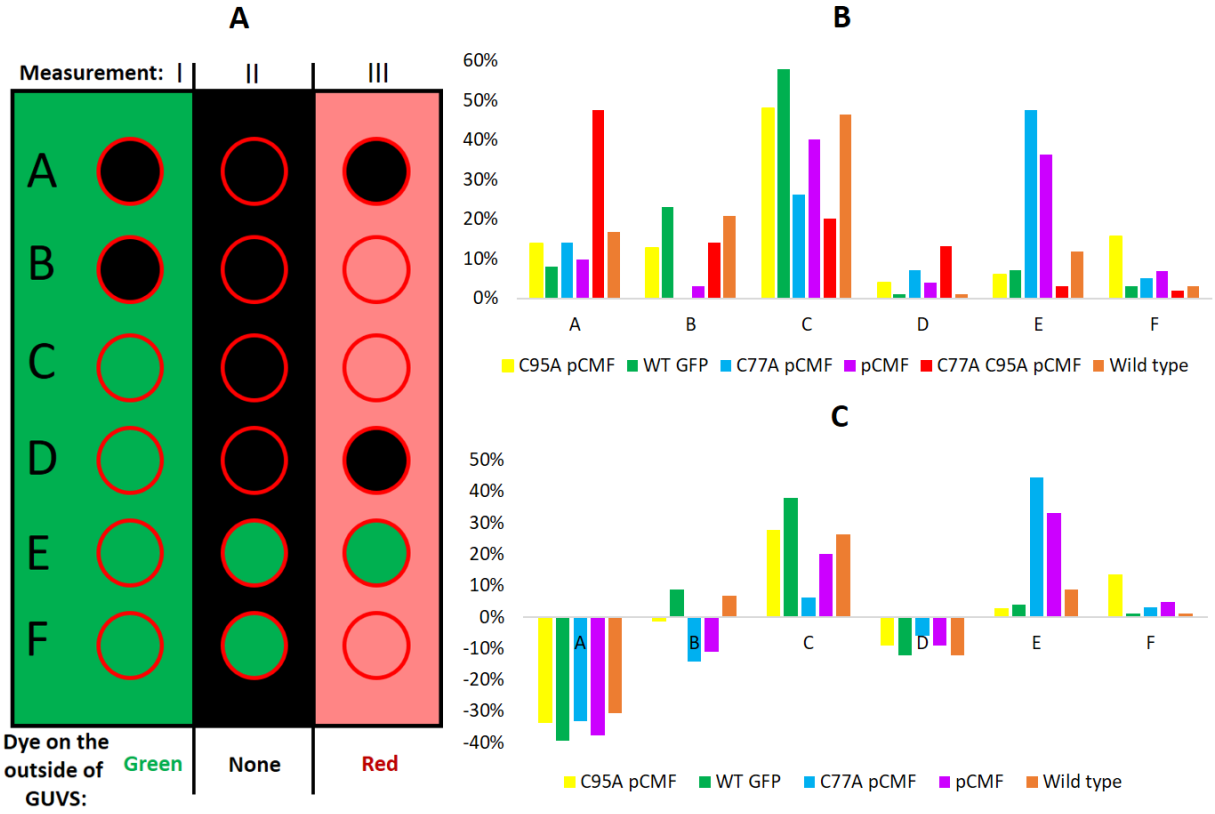

Figure 15. GUVs divided into groups based on pore opening dynamics and stability as determined by DLSGA. A: *graphical representation of GUVs belonging to groups A-F during measurements I-III.* ***B:*** *graphical representation of GUV distribution across all groups for each FGF2 variant that was measured using small fluorescent dyes – Alexa fluor 532 and 647.* ***C:*** *graphical representation of GUV distribution across all groups for FGF2 variants. In this graph, C77A C95A pCMF was used as a blank and its group populations were subtracted from the data for the other variants. Negative populations in this graph signify that the blank had higher population for that group than the FGF2 variant with negative group population. Both graded and all or none leakage was used to divide GUVs into groups.*

Group B are GUVs that became leaky later in the experiment, specifically after the excess protein was washed out from the bulk and binding of additional FGF2 to the GUVs is highly unlikely. The removal of excess FGF2 causes shift in equilibrium between membrane-bound FGF2 and free FGF2, which can only lead to decrease in the amount of membrane-bound FGF2. For this reason it was expected that there would be less GUVs containing the red dye (which is added after removal of excess FGF2) than the green dye (added before removal of excess FGF2) in measurement III. Surprisingly, this is only true for pCMF, C77A pCMF and C77A C95A pCMF variants (**Table 6**). The fact that more GUVs became leaky after the decrease of membrane-bound FGF2 could be simply attributed to increased number of membrane defects due to ageing. However, that would not explain why group B is populated (after the blank was subtracted) only for some of the FGF2 variants. In fact, group B is populated specifically for non-phosphorylated variants. This could be explained by the fact that phosphorylated Y81 makes required time for pore-formation shorter. Therefore, in its absence some pores form at later stages of the experiment. This means that even after the removal of unbound protein from the bulk and the subsequent shift in equilibrium enough FGF2 remains bound to membrane to form new pores on intact GUVs.

Group C are GUVs that were leaky at least for some time during all three steps that were measured. To explain the significance of this group, it is important to consider that the third phase of the unconventional translocation mechanism of FGF2 was not observed in these experiments. FGF2 can form pores on the membrane but it cannot pass through efficiently. This means that successful pore-opening does not lead to pore-closing as it would *in vivo.* Therefore, successful pore-formation leads to stable pores. After the subtraction of the blank, all variants still show positive populations of group C (**Figure 15C**). C77A pCMF variant populates the group C to a lesser extent than the other variants; this means that despite being able to form higher oligomers it cannot form stable pores. This suggests that C77 plays an important role in the FGF2 pore-formation. In comparison, C95A pCMF variant populates the group C to a similar extent as non-mutated FGF2 variants despite the fact that it can only form dimers. In chapter 2.10 TIRF microscopy FGF2 experiments on cells were mentioned. (107) In these experiments mostly FGF2 dimers were detected on membrane as translocation was occurring. Based on that, a hypothesis was proposed that these dimers were important intermediates for formation of higher oligomeric states that then undergo translocation, but are too unstable to be detected. However, these results could also be interpreted differently – mostly dimers were detected because only dimers are required for translocation across membrane. This would

explain our results for C95A pCMF and C77A pCMF variants – the variant that only forms dimers performed considerably better in terms of formation of stable pores than the one that can form higher oligomers. The inability of C77A pCMF variant to utilize C77-C77 disulfide bridges significantly impacted its ability to form stable pores. This points to the possibility that dimers formed by C77-C77 disulfide bridges are the main form of FGF2 that performs translocation across cellular membrane.

Group D are GUVs whose pores closed after the excess protein was removed from the bulk and did not open after the red dye was added. This scenario could be explained by destabilization of pores caused by the shift in equilibrium after the removal of free FGF2. After the subtraction of the blank, all remaining FGF2 variants show negative group D population, therefore, this effect is insignificant. Decrease of membrane-bound FGF2 does not significantly hinder formation of new pores (positive group B population), nor does it lead to closing of old pores (insignificant group D population). If dimers are the oligomers responsible for formation of stable pores then perhaps even a few FGF2 molecules bound to a GUV can suffice for pore formation. This could explain the insignificant influence of decrease of membrane-bound FGF2 on pore formation.

Group E are GUVs whose pores closed even before the excess protein was removed and never opened again. This group is highly populated in case of pCMF and C77A pCMF variants. GUVs that belong to this population are often leaked only slightly (low intensity of green dye on the inside of the GUV – graded leakage). This means that the membrane was permeabilized only for a short moment and no stable pores were formed. This probably happens as a result of membrane destabilization when FGF2 oligomers are inserted into the membrane. However, in the case of these two variants, this often does not lead to successful pore formation. For the C77A mutant, it could be again explained by the hypothesis that C77-C77 disulfide bridge is crucial for formation of stable pores, as mentioned above. In case of the nonmutated pCMF variant, the reason is unclear.

GUVs belonging to group F are those that were leaky for a part of the time when the green dye was present in the bulk, but then their pores closed before the dye and the excess protein were removed from the bulk. However, after the second dye was added, they became leaky again. This group could simply be explained as GUVs from group E that became leaky due to membrane defects from ageing when the red dye was present. But this would not explain why C95A pCMF has significant population of GUVs in this group. C95A pCMF forms mostly only dimers, these dimers can form stable pores but they cannot form higher oligomerization states

which could in theory further stabilize a pore that was formed by a dimer. This would suggest a scenario where unstable pores form at the start then disappear and then appear again later as only two FGF2 molecules with good orientation are required for pore formation.

5.3. Double leakage single GUV assay with 4 KDa dextran dyes

To learn more about the size of membrane pores, we decided to carry out the same series of experiments with larger fluorescent dyes. Previous experiments with FGF2 showed that 3 KDa dyes can pass through FGF2 pores and 10 KDa cannot (99). For this reason, 4 KDa dextrans were chosen as their hydrodynamic radius could be similar to the actual pore radius. This assumption was proven correct as there was significant decrease in leakage (**Table 7**) as compared to small dyes (**Table 6**). This difference was especially notable for all or none leakage which requires a pore of a sufficient size to be open for a long time. It has been shown for another pore-forming protein (Bax α5) that the pore size can decrease in time as the pore relaxes after its formation. (118) It is possible that at the time of the pore-formation the pore radius is large enough to let the dextran dyes through. But the radius then quickly decreases, not allowing for the concentration of the dye on the inside and on the outside of the GUVs to equilibrate. This is not the case for FGF2-GFP variant, however. This suggests that GFP domain either increases the FGF2 pore size or somehow prevents the relaxion of the pore. GFP (26.9 KDa) fused to FGF2 (18 KDa) makes the fusion protein significantly bigger than normal FGF2 and stable pores form by insertion of FGF2 oligomers into the membrane. For these reasons, it is not surprising that GFP domain can affect pore size. Double cysteine mutant exhibited the lowest leakage and was used as the blank for further analysis. (**Figure 16**)

Based on these results the pore size was roughly estimated by assuming that dextran dye molecules are perfect spheres with the same density as water (during the experiments they were in HEPES buffer). These simple equations were utilized:

$$V = \frac{M_w(FITC - dextran)}{\rho_{water,25°C} \cdot N_A}$$

$$V = \frac{4\pi r^3}{3},$$

(17,18)

where V is volume of dextran particle, ρ is density, N_A is Avogadro constant and r is radius.

The estimated diameter of FGF2 pores is 2.34 nm assuming the pore is circular and exactly matches the estimated size of FITC-dextran particle.

Table 7. Double leakage single GUV assay results for six variants of FGF2 using PM2 membrane composition. *Fractions of leaky GUVs containing dextran fluorescent dyes – TRITC-dextran 4 KDa and FITC-dextran 4 KDa. Both types of leakage were observed. Total leakage represents sum of fractions for both types of leakage.*

FGF2 variant	Wild type	PCMF	FGF2-GFP	C77A PCMF	C95A PCMF	C77A C95A PCMF
Types of leakage	**All or none; graded; total**					
Percentage of GUVs containing TRITC dextran 4 KDa, measurement I	9%; 19%; 28%	11%; 17%; 28%	24%; 8%; 32%	3%; 20%; 23%	5%; 24%; 29%	9%; 4%; 13%
Percentage of GUVs containing TRITC dextran 4 KDa, measurement II	1%; 16%; 17%	1%; 16%; 17%	1%; 5%; 6%	1%; 18%; 19%	1%; 25%; 26%	0%; 5%; 5%
Percentage of GUVs containing TRITC dextran 4 KDa, measurement III	1%; 5%; 6%	1%; 10%; 11%	1%; 5%; 6%	1%; 11%; 12%	1%; 19%; 20%	0%; 4%; 4%
Percentage of GUVs containing FITC dextran 4 KDa, measurement III	12%; 21%; 33%	12%; 9%; 21%	36%; 5%; 41%	5%; 14%; 19%	6%; 5%; 11%	12%; 3%; 15%
Percentage of GUVs containing either green or blue dye, measurement III	13%; 26%; 39%	13%; 19%; 31%	37%; 10%; 47%	6%; 25%; 29%	7%; 24%; 31%	12%; 7%; 19%

GUVs were divided into groups based on pore opening dynamics and stability (**Figure 16**). The inability to form sufficiently large pores for a longer period of time is also apparent from low C populations for all variants except FGF2-GFP. The other variants behaved similarly having high A populations (**Figure 16B**). The differences between variants are relatively small and hard to interpret due to low portion of GUVs with big enough pores to let dextran dyes through.

Positive group B population for FGF2-GFP variant is consistent with the results for small dyes, where non-pCMF variants have been shown to form stable pores at later times. There is slightly positive population also for wild type FGF2, but to smaller degree than for FGF2-GFP which supports the hypothesis of GFP impacting the pore-size.

Insignificant group D populations are also consistent with results for small dyes. For discussion about group D see the previous chapter.

Group E is significantly populated by the pCMF variants while non-phosphorylated variants do not populate group E. This makes sense as phosphorylated Y81 (which is the meaning of pCMF) is known to stimulate membrane insertion of FGF2 oligomers (90,99,105), as mentioned above. Therefore, it is also logical that pCMF variants have significant populations of GUVs that are leaky in the earliest measurement (groups C,E,F). However, due to the inability to form stable pores that are large enough for 4 KDa dextran molecules to pass through, populations of group C are low. Group E are probably GUVs that formed pores which relaxed to smaller pore size quickly after formation. This has been known to happen in case of Bax α5 pores (118).

Group F similarly to group B are GUVs that formed pores after the removal of unbound FGF2 from the system. However, in case of group F, these GUVs were also leaky when the first dye was present in the bulk. This can be explained similarly to group E, early in the experiment, the GUVs became leaky and the pore size decreased. Because of this, the green dye stayed inside of these GUVs after the removal of the dye from the imaging chamber. After addition of the second dye into the imaging chamber, new pores formed on some of these GUVs. This is more pronounced for the wild type FGF2 for two reasons. Firstly, it is not phosphorylated which results in the tendency to form new pores later in the experiment. Secondly, it is not fused with GFP which means that the pores that formed when the first dye was present relaxed to insufficient size to allow passage of 4 KDa dextran.

Overall, the experiments with 4 KDa dextran dyes did not provide much new insight into the differences between FGF2 variants (aside from the influence of GFP on the pore size). The results for the other variants do not reveal anything that was not already apparent from the experiments with small dyes. This supports the conclusions that were made based on small dye experiments in regards to role of pCMF, C77 and C95. On the other hand, dextran experiments allowed for rough estimation of the size of FGF2 pores. This estimate could be improved by employing other experimental techniques.

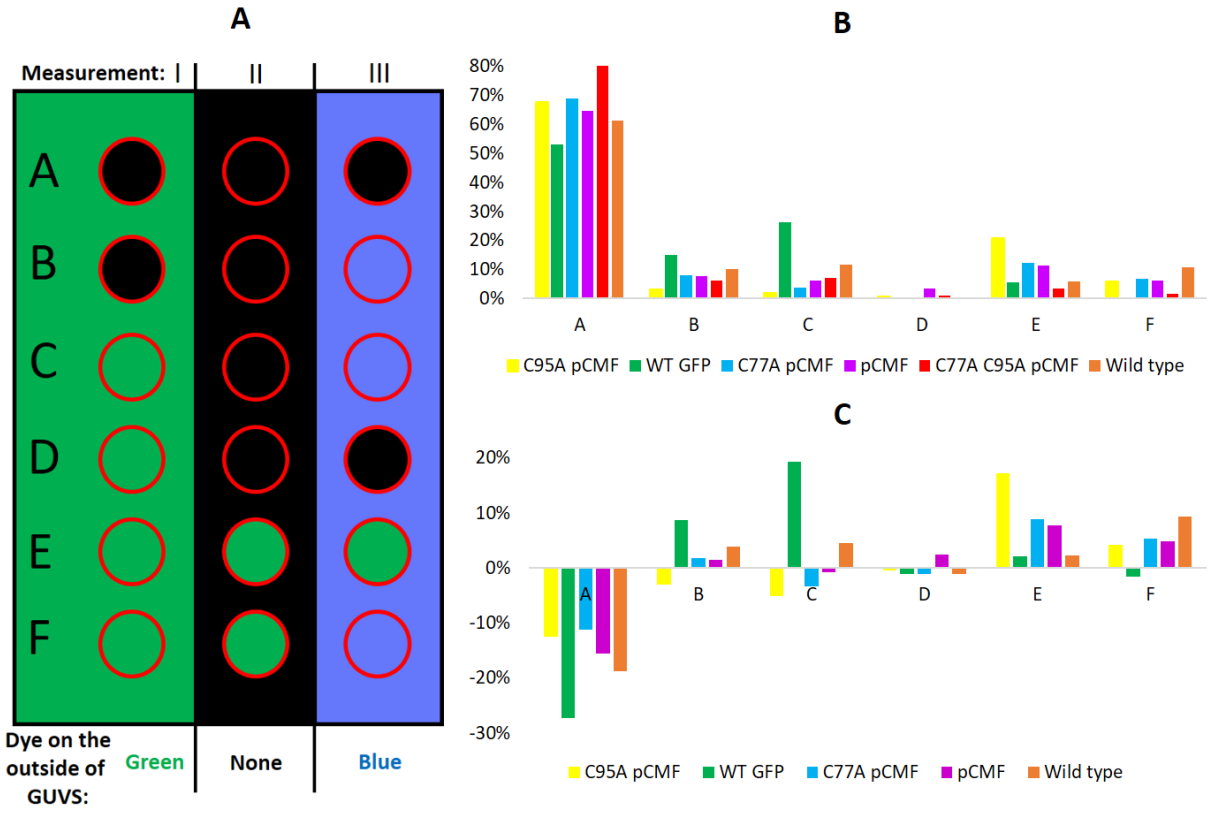

Figure 16. GUVs divided into groups based on pore opening dynamics and stability as determined by DLSGA. ***A:*** *graphical representation of GUVs belonging to groups A-F during all three measurements.* ***B:*** *graphical representation of group distribution across all groups for each FGF2 variant that was measured using 4 KDa dextran fluorescent dyes – TRITC-dextran and FITC-dextran.* ***C****: graphical representation of group distribution across all groups for each FGF2 variant. In this graph, C77A C95A pCMF was used as a blank and its group populations were subtracted from the data for the other variants. Negative populations in this graph signify that the blank had higher population for that group than the FGF2 variant with negative group population. Both graded and all or none leakage was used to divide GUVs into groups.*

6. Conclusions

The aims of this thesis were to 1) develop a simple fluorescence microscopy method to investigate the dynamics of pore-formation in detail and 2) to apply this method to study formation of membrane pores by FGF2 protein. We successfully established the double leakage single GUV assay (DLSGA) at the department of Biophysical Chemistry, Heyrovsky Institute and applied this new approach to study formation of FGF2 pores. By doing this, it became apparent that the method is suitable to characterize pore-formation in real time, thus providing insights into structure-function relationship of FGF2 elements. The method was able to elucidate the importance of C77 compared to C95 for the formation of pores. This was achieved by tracking differences in membrane permeabilization on large number of individual GUVs for FGF2 variants that had either C77 or C95 replaced by alanin. This information was then used in conjunction with determined oligomeric states of FGF2 C95A variant and FGF2 C77A variant and recent *in vivo* experiments which revealed the importance of FGF2 dimers for the unconventional FGF2 mechanism of translocation across the cellular membrane. The results in this thesis show that both higher oligomer species of FGF2 and FGF2 dimers are capable of formation of stable FGF2 pores. However, FGF2 C77A variant which cannot utilize C77-C77 disulfide bridges but can form higher oligomer species has its ability to form stable pores significantly diminished.

Furthermore, when double leakage single GUV assay was performed using 4 KDa fluorescent dextran dyes, it revealed that the GFP fused to FGF2, which has been largely used in many studies, influences the size of FGF2 pores. This was demonstrated by the fact that the other FGF2 variants which were not fused to GFP were unable to form pores that would enable continuous passage of dextran dyes. Based on these results, we were also able to estimate the size of FGF2 pores. However, besides the influence of GFP, we were unable to determine with certainty if cysteine mutations or phosphorylation of Y81 influence the pore size.

Since the key molecules that enable effective translocation were missing in our experimental setup, we could not study the final phase of FGF2 translocation, i.e. unbinding of FGF2 from the inner membrane leaflet. This could be mitigated in the future by either including these molecules in DLSGA experiments or performing experiments on cells with single cysteine mutants. This would give greater credibility to conclusions drawn from the results in this thesis.

The power of this new method lies in its simplicity – it does not require cells or FCS setup to produce impactful results, especially when used in tandem with other methods. It is also well

suited to study structure-function relationship by using mutated or otherwise modified variants of pore-forming proteins. Because it can provide detailed information about pore-formation dynamics, even small differences between variants can be detected by this single GUV confocal fluorescence microscopy method.

7. Literature

1. Albarracin G. Bernard Valeur Molecular Fluorescence Principles and Applications.

2. Franck J, Dymond EG. Elementary processes of photochemical reactions. Trans Faraday Soc. 1926 Jan 1;21(February):536–42.

3. Condon E. A Theory of Intensity Distribution in Band Systems. Phys Rev. 1926 Dec 1;28(6):1182–201.

4. Atkins PW, Friedman R. Molecular quantum mechanics. 5th ed. Oxford ; New York: Oxford University Press; 2011. 537 p.

5. Chmyrov A. Photo-induced dark states in fluorescence spectroscopy – investigations & applications. 2010.

6. Kasha M. Characterization of electronic transitions in complex molecules. Discuss Faraday Soc. 1950 Jan 1;9(0):14–9.

7. Stokes GG. On the Change of Refrangibility of Light. Philos Trans R Soc Lond. 1852;142:463–562.

8. Schweizer T, Kubach H, Koch T. Investigations to characterize the interactions of light radiation, engine operating media and fluorescence tracers for the use of qualitative light-induced fluorescence in engine systems. Automot Engine Technol. 2021 Dec 1;6:1–13.

9. P. S. Molecular spectroscopy of the triplet state . S.P. McGlynn, T. Azumi and M. Kkinoshita, Prentice-Hall International, Hemel Hemptead (U.K.), 1969, pp. J Mol Struct. 1972 May 1;12:310–310.

10. Ketsle GA, Levshin LV, Bryukhanov VV. Mechanism of the external heavy atom effect on intersystem crossing in rhodamine dye solutions. J Appl Spectrosc. 1976 May 1;24(5):573–7.

11. Kasha M. Collisional Perturbation of Spin-Orbital Coupling and the Mechanism of Fluorescence Quenching. A Visual Demonstration of the Perturbation. J Chem Phys. 1952 Jan 1;20:71–4.

12. Hoijtink GJ. The influence of paramagnetic molecules on singlet-triplet transitions. Mol Phys. 1960 Jan 1;3(1):67–70.

13. Widengren J, Seidel CAM. Manipulation and characterization of photo-induced transient states of Merocyanine 540 by fluorescence correlation spectroscopy. Phys Chem Chem Phys. 2000 Jan 1;2(15):3435–41.

14. Ringemann C, Schönle A, Giske A, von Middendorff C, Hell SW, Eggeling C. Enhancing Fluorescence Brightness: Effect of Reverse Intersystem Crossing Studied by Fluorescence Fluctuation Spectroscopy. ChemPhysChem. 2008;9(4):612–24.

15. Lakowicz J. Lakowicz JR (2006) Principles of fluorescence spectroscopy, 3rd edn. Springer, New York, 2006. 2006.

16. Lark-Horovitz K. Fluorescence and Phosphorescence. Peter Pringsheim. New York-London: Interscience, 1949. 794 pp. $15.00.; An Introduction to Luminescence of Solids. Humboldt W. Leverenz. London: Chapman & Hall; New York: John Wiley, 1950. 569 pp. $12.00. Science. 1950 Apr 21;111(2886):410–2.

17. Drexhage KH. 5. Structure and properties of laser dyes. In: Schäfer FP, editor. Dye Lasers Berlin, Heidelberg: Springer; 1990. p. 155–200. (Topics in Applied Physics). Available from: https://doi.org/10.1007/3-540-51558-5_11

18. Zwischenmolekulare Energiewanderung und Fluoreszenz - Förster - 1948 - Annalen der Physik - Wiley Online Library

19. Clegg RM. Fluorescence resonance energy transfer and nucleic acids. Methods Enzymol. 1992;211:353–88.

20. Jares-Erijman EA, Jovin TM. FRET imaging. Nat Biotechnol. 2003 Nov;21(11):1387–95.

21. Roy R, Hohng S, Ha T. A practical guide to single-molecule FRET. Nat Methods. 2008 Jun;5(6):507–16.

22. Schuler B, Eaton WA. Protein folding studied by single-molecule FRET. Curr Opin Struct Biol. 2008 Feb;18(1):16–26.

23. Matthews DR, Carlin LM, Ofo E, Barber PR, Vojnovic B, Irving M, et al. Time-lapse FRET microscopy using fluorescence anisotropy. J Microsc. 2010 Jan;237(1):51–62.

24. Koukalová A, Amaro M, Aydogan G, Gröbner G, Williamson PTF, Mikhalyov I, et al. Lipid Driven Nanodomains in Giant Lipid Vesicles are Fluid and Disordered. Sci Rep. 2017 Jul 14;7(1):5460.

25. Chandra AK, Turro NJ, Lyons AL, Stone P. The intramolecular external heavy atom effect in bromo-, benzo-, and naphthonorbornenes. J Am Chem Soc. 1978 Aug 1;100(16):4964–8.

26. Solov'ev KN, Borisevich EA. Intramolecular heavy-atom effect in the photophysics of organic molecules. Phys-Uspekhi. 2005 Mar 31;48(3):231.

27. Rae M, Fedorov A, Berberan-Santos MN. Fluorescence quenching with exponential distance dependence: Application to the external heavy-atom effect. J Chem Phys. 2003;119(4):2223.

28. Levshin LV, Nizamov N. Concentration quenching of the luminescence of rhodamine dyes in binary solvents. J Appl Spectrosc. 1966 Dec 1;5(6):531–4.

29. Kelkar VK, Valaulikar BS, Kunjappu JT, Manohar C. Aggregation Characteristics of Laser Dye Rhodamine 6g in Aqueous Surfactant Solutions. Photochem Photobiol. 1990;52(4):717–21.

30. Yuzhakov V. Aggregation of dye molecules and its influence on the spectral luminescent properties of solutions. Russ Chem Rev. 2007 Oct 17;61:613.

31. Bergström F, Mikhalyov I, Hägglöf P, Wortmann R, Ny T, Johansson LBÅ. Dimers of Dipyrrometheneboron Difluoride (BODIPY) with Light Spectroscopic Applications in Chemistry and Biology. J Am Chem Soc. 2002 Jan 1;124(2):196–204.

32. Eftink MR, Ghiron CA. Fluorescence quenching studies with proteins. Anal Biochem. 1981 Jul 1;114(2):199–227.

33. Zhuang X, Ha T, Kim HD, Centner T, Labeit S, Chu S. Fluorescence quenching: A tool for single-molecule protein-folding study. Proc Natl Acad Sci U S A. 2000 Dec 19;97(26):14241–4.

34. Yang H, Luo G, Karnchanaphanurach P, Louie TM, Rech I, Cova S, et al. Protein conformational dynamics probed by single-molecule electron transfer. Science. 2003 Oct 10;302(5643):262–6.

35. Seidel CAM. Nucleic acid base specific quenching of coumarin-120-derivative in nucleotid-conjugates-photoinduced electron transfer. In: Birge RR, Nafie LA, editors. Los Angeles, CA; 1991

36. Seidel CAM, Schulz A, Sauer MHM. Nucleobase-Specific Quenching of Fluorescent Dyes. 1. Nucleobase One-Electron Redox Potentials and Their Correlation with Static and Dynamic Quenching Efficiencies. J Phys Chem. 1996 Jan 1;100(13):5541–53.

37. Bonnet G, Krichevsky O, Libchaber A. Kinetics of conformational fluctuations in DNA hairpin-loops. Proc Natl Acad Sci U S A. 1998 Jul 21;95(15):8602–6.

38. Eggeling C, Fries JR, Brand L, Günther R, Seidel CAM. Monitoring conformational dynamics of a single molecule by selective fluorescence spectroscopy. Proc Natl Acad Sci. 1998 Feb 17;95(4):1556–61.

39. Zhu P, Clamme JP, Deniz AA. Fluorescence Quenching by TEMPO: A Sub-30 Å Single-Molecule Ruler. Biophys J. 2005 Nov;89(5):L37–9.

40. Widengren J, Rigler R. Mechanisms of photobleaching investigated by fluorescence correlation spectroscopy. Bioimaging. 2001 May 25;4:149–57.

41. Dittrich PS, Schwille P. Photobleaching and stabilization of. fluorophores used for single-molecule analysis. with one- and two-photon excitation. Appl Phys B Lasers Opt. 2001 Dec 1;73:829–37.

42. Yeow EKL, Melnikov SM, Bell TDM, De Schryver FC, Hofkens J. Characterizing the fluorescence intermittency and photobleaching kinetics of dye molecules immobilized on a glass surface. J Phys Chem A. 2006 Feb 9;110(5):1726–34.

43. Vogelsang J, Kasper R, Steinhauer C, Person B, Heilemann M, Sauer M, et al. A reducing and oxidizing system minimizes photobleaching and blinking of fluorescent dyes. Angew Chem Int Ed Engl. 2008;47(29):5465–9.

44. Eggeling C, Widengren J, Rigler R, Seidel CA. Photobleaching of Fluorescent Dyes under Conditions Used for Single-Molecule Detection: Evidence of Two-Step Photolysis. Anal Chem. 1998 Jul 1;70(13):2651–9.

45. Eggeling C, Volkmer A, Seidel C. Molecular Photobleaching Kinetics of Rhodamine 6G by One- and Two-Photon Induced Confocal Fluorescence Microscopy. Chemphyschem Eur J Chem Phys Phys Chem. 2005 May 13;6:791–804.

46. Wilkinson F. Quenching of electronically excited states by molecular oxygen in fluid solution. Pure Appl Chem. 1997 Jan 1;69(4):851–6.

47. Kawaoka K, Khan AU, Kearns DR. Role of Singlet Excited States of Molecular Oxygen in the Quenching of Organic Triplet States. J Chem Phys. 1967 Mar;46(5):1842–53.

48. Hübner CG, Renn A, Renge I, Wild UP. Direct observation of the triplet lifetime quenching of single dye molecules by molecular oxygen. J Chem Phys. 2001 Dec;115(21):9619–22.

49. Davies MJ. Reactive species formed on proteins exposed to singlet oxygen. Photochem Photobiol Sci. 2004 Jan 14;3(1):17–25.

50. Sies H, Menck CFM. Singlet oxygen induced DNA damage. Mutat Res. 1992 Sep 1;275(3):367–75.

51. Rasnik I, McKinney SA, Ha T. Nonblinking and long-lasting single-molecule fluorescence imaging. Nat Methods. 2006 Nov;3(11):891–3.

52. Widengren J, Chmyrov A, Eggeling C, Löfdahl PA, Seidel CAM. Strategies to improve photostabilities in ultrasensitive fluorescence spectroscopy. J Phys Chem A. 2007 Jan 25;111(3):429–40.

53. Aitken CE, Marshall RA, Puglisi JD. An oxygen scavenging system for improvement of dye stability in single-molecule fluorescence experiments. Biophys J. 2008 Mar 1;94(5):1826–35.

54. Axelrod D, Koppel DE, Schlessinger J, Elson E, Webb WW. Mobility measurement by analysis of fluorescence photobleaching recovery kinetics. Biophys J. 1976 Sep;16(9):1055–69.

55. Meyvis TK, De Smedt SC, Van Oostveldt P, Demeester J. Fluorescence recovery after photobleaching: a versatile tool for mobility and interaction measurements in pharmaceutical research. Pharm Res. 1999 Aug;16(8):1153–62.

56. White J, Stelzer E. Photobleaching GFP reveals protein dynamics inside live cells. Trends Cell Biol. 1999 Feb 1;9(2):61–5.

57. Lippincott-Schwartz J, Snapp E, Kenworthy A. Studying protein dynamics in living cells. Nat Rev Mol Cell Biol. 2001 Jun;2(6):444–56.

58. Carman C. Overview: Imaging in the Study of Integrins. Methods Mol Biol Clifton NJ. 2012 Jan 1;757:159–89.

59. Schäfer FP. 1. Principles of dye laser operation. In: Schäfer FP, editor. Dye Lasers. Berlin, Heidelberg: Springer; 1990. p. 1–89. (Topics in Applied Physics). Available from: https://doi.org/10.1007/3-540-51558-5_7

60. Yadav LDS. Organic Spectroscopy. Dordrecht: Springer Netherlands; 2005

61. Hell SW, Wichmann J. Breaking the diffraction resolution limit by stimulated emission: stimulated-emission-depletion fluorescence microscopy. Opt Lett. 1994 Jun 1;19(11):780–2.

62. Hell SW. Far-field optical nanoscopy. Science. 2007 May 25;316(5828):1153–8.

63. Rust MJ, Bates M, Zhuang X. Sub-diffraction-limit imaging by stochastic optical reconstruction microscopy (STORM). Nat Methods. 2006 Oct;3(10):793–6.

64. Betzig E, Patterson GH, Sougrat R, Lindwasser OW, Olenych S, Bonifacino JS, et al. Imaging intracellular fluorescent proteins at nanometer resolution. Science. 2006 Sep 15;313(5793):1642–5.

65. Carlsson K, Åslund N. Confocal imaging for 3-D digital microscopy. Appl Opt. 1987 Aug 15;26(16):3232–8.

66. Carlsson K, Danielsson PE, Lenz R, Liljeborg A, Majlöf L, Åslund N. Three-dimensional microscopy using a confocal laser scanning microscope. Opt Lett. 1985 Feb 1;10(2):53–5.

67. White JG, Amos WB, Fordham M. An evaluation of confocal versus conventional imaging of biological structures by fluorescence light microscopy. J Cell Biol. 1987 Jul;105(1):41–8.

68. Hecht E. Optics. Reading, Mass.: Addison-Wesley; 2002.

69. Rayleigh, Lord. On the Theory of Optical Images, with special reference to the Microscope. J R Microsc Soc. 1903;23(4):474–82.

70. Bertocchi C, Goh W, Zhang Z, Kanchanawong P. Nanoscale Imaging by Superresolution Fluorescence Microscopy and Its Emerging Applications in Biomedical Research. Crit Rev Biomed Eng. 2013 Jan 1;41:281–308.

71. Bikfalvi A, Klein S, Pintucci G, Rifkin DB. Biological roles of fibroblast growth factor-2. Endocr Rev. 1997 Feb;18(1):26–45.

72. Grothe C, Nikkhah G. The role of basic fibroblast growth factor in peripheral nerve regeneration. Anat Embryol (Berl). 2001 Sep 1;204(3):171–7.

73. Washio A, Teshima H, Yokota K, Kitamura C, Tabata Y. Preparation of gelatin hydrogel sponges incorporating bioactive glasses capable for the controlled release of fibroblast growth factor-2. J Biomater Sci Polym Ed. 2019 Jan 2;30(1):49–63.

74. Xuan X, Zhou Y, Chen A, Zheng S, An Y, He H, et al. Silver crosslinked injectable bFGF-eluting supramolecular hydrogels speed up infected wound healing. J Mater Chem B. 2020 Feb 19;8(7):1359–70.

75. Lou Z, Huang P, Yang J, Xiao J, Chang J. Direct application of bFGF without edge trimming on human subacute tympanic membrane perforation. Am J Otolaryngol. 2016 Mar 1;37(2):156–61.

76. Kanemaru SI, Umeda H, Kitani Y, Nakamura T, Hirano S, Ito J. Regenerative Treatment for Tympanic Membrane Perforation. Otol Neurotol. 2011 Oct;32(8):1218–23.

77. Lou ZC, Wang YBZ. Healing outcomes of large (>50%) traumatic membrane perforations with inverted edges following no intervention, edge approximation and fibroblast growth factor application; a sequential allocation, three-armed trial. Clin Otolaryngol. 2013;38(4):289–96.

78. Lou ZC, He JG. A randomised controlled trial comparing spontaneous healing, gelfoam patching and edge-approximation plus gelfoam patching in traumatic tympanic membrane perforation with inverted or everted edges. Clin Otolaryngol Off J ENT-UK Off J Neth Soc Oto-Rhino-Laryngol Cervico-Facial Surg. 2011 Jun;36(3):221–6.

79. Noh KH, Kim SH, Kim JH, Song KH, Lee YH, Kang TH, et al. API5 Confers Tumoral Immune Escape through FGF2-Dependent Cell Survival Pathway. Cancer Res. 2014 Jun 30;74(13):3556–66.

80. Sliutz G, Tempfer C, Obermair A, Reinthaller A, Gitsch G, Kainz C. Serum Evaluation of Basic Fibroblast Growth-Factor in Cervical-Cancer Patients. Cancer Lett. 1995 Aug 1;94(2):227–31.

81. Obermair A, Speiser P, Reisenberger K, Ullrich R, Czerwenka K, Kaider A, et al. Influence of intratumoral basic fibroblast growth factor concentration on survival in ovarian cancer patients. Cancer Lett. 1998 Aug 14;130(1–2):69–76.

82. Ohta T, Yamamoto M, Numata M, Iseki S, Tsukioka Y, Miyashita T, et al. Expression of Basic Fibroblast Growth-Factor and Its Receptor in Human Pancreatic Carcinomas. Br J Cancer. 1995 Oct;72(4):824–31.

83. FGF-2 protects small cell lung cancer cells from apoptosis through a complex involving PKCε, B-Raf and S6K2. EMBO J. 2006 Jul 12;25(13):3078–88.

84. Kato J, Wanebo H, Calabresi P, Clark J. Basic Fibroblast Growth-Factor Production and Growth-Factor Receptors as Potential Targets for Melanoma Therapy. Melanoma Res. 1992 May;2(1):13–23.

85. Sommer A, Moscatelli D, Rifkin DB. An amino-terminally extended and post-translationally modified form of a 25kD basic fibroblast growth factor. Biochem Biophys Res Commun. 1989 May 15;160(3):1267–74.

86. Sommer A, Brewer MT, Thompson RC, Moscatelli D, Presta M, Rifkin DB. A form of human basic fibroblast growth factor with an extended amino terminus. Biochem Biophys Res Commun. 1987 Apr 29;144(2):543–50.

87. Quarto N, Finger FP, Rifkin DB. The NH2-terminal extension of high molecular weight bFGF is a nuclear targeting signal. J Cell Physiol. 1991 May;147(2):311–8.

88. Dono R, James D, Zeller R. A GR-motif functions in nuclear accumulation of the large FGF-2 isoforms and interferes with mitogenic signalling. Oncogene. 1998 Apr 23;16(16):2151–8.

89. Bugler B, Amalric F, Prats H. Alternative initiation of translation determines cytoplasmic or nuclear localization of basic fibroblast growth factor. Mol Cell Biol. 1991 Jan;11(1):573–7.

90. La Venuta G, Wegehingel S, Sehr P, Müller HM, Dimou E, Steringer JP, et al. Small Molecule Inhibitors Targeting Tec Kinase Block Unconventional Secretion of Fibroblast Growth Factor 2. J Biol Chem. 2016 Aug 19;291(34):17787–803.

91. Nickel W. The Unconventional Secretory Machinery of Fibroblast Growth Factor 2. Traffic. 2011;12(7):799–805.

92. Nickel W, Rabouille C. Mechanisms of regulated unconventional protein secretion. Nat Rev Mol Cell Biol. 2009 Feb;10(2):148–55.

93. Rabouille C, Malhotra V, Nickel W. Diversity in unconventional protein secretion. J Cell Sci. 2012 Nov 15;125(22):5251–5.

94. Christensen PU, Davey J, Nielsen O. The Schizosaccharomyces pombe mam1 gene encodes an ABC transporter mediating secretion of M-factor. Mol Gen Genet MGG. 1997 Jun 1;255(2):226–36.

95. McGrath JP, Varshavsky A. The yeast STE6 gene encodes a homologue of the mammalian multidrug resistance P-glycoprotein. Nature. 1989 Aug;340(6232):400–4.

96. Andrei C, Dazzi C, Lotti L, Torrisi MR, Chimini G, Rubartelli A. The Secretory Route of the Leaderless Protein Interleukin 1β Involves Exocytosis of Endolysosome-related Vesicles. Mol Biol Cell. 1999 May;10(5):1463–75.

97. Kinseth MA, Anjard C, Fuller D, Guizzunti G, Loomis WF, Malhotra V. The Golgi-Associated Protein GRASP Is Required for Unconventional Protein Secretion during Development. Cell. 2007 Aug 10;130(3):524–34.

98. Grieve AG, Rabouille C. Golgi Bypass: Skirting Around the Heart of Classical Secretion. Cold Spring Harb Perspect Biol. 2011 Jan 4;3(4):a005298.

99. Steringer JP, Bleicken S, Andreas H, Zacherl S, Laussmann M, Temmerman K, et al. Phosphatidylinositol 4,5-bisphosphate (PI(4,5)P2)-dependent oligomerization of fibroblast growth factor 2 (FGF2) triggers the formation of a lipidic membrane pore implicated in unconventional secretion. J Biol Chem. 2012 Aug 10;287(33):27659–69.

100. Venuta GL, Zeitler M, Steringer JP, Müller HM, Nickel W. The Startling Properties of Fibroblast Growth Factor 2: How to Exit Mammalian Cells without a Signal Peptide at Hand *. J Biol Chem. 2015 Nov 6;290(45):27015–20.

101. Brough D, Pelegrin P, Nickel W. An emerging case for membrane pore formation as a common mechanism for the unconventional secretion of FGF2 and IL-1β. J Cell Sci. 2017 Oct 1;130(19):3197–202.

102. Temmerman K, Ebert AD, Müller HM, Sinning I, Tews I, Nickel W. A Direct Role for Phosphatidylinositol-4,5-bisphosphate in Unconventional Secretion of Fibroblast Growth Factor 2. Traffic. 2008;9(7):1204–17.

103. Steringer JP, Lange S, Čujová S, Šachl R, Poojari C, Lolicato F, et al. Key steps in unconventional secretion of fibroblast growth factor 2 reconstituted with purified components. Burd CG, editor. eLife. 2017 Jul 19;6:e28985.

104. Zacherl S, La Venuta G, Müller HM, Wegehingel S, Dimou E, Sehr P, et al. A direct role for ATP1A1 in unconventional secretion of fibroblast growth factor 2. J Biol Chem. 2015 Feb 6;290(6):3654–65.

105. Ebert AD, Laussmann M, Wegehingel S, Kaderali L, Erfle H, Reichert J, et al. Tec-kinase-mediated phosphorylation of fibroblast growth factor 2 is essential for unconventional secretion. Traffic Cph Den. 2010 Jun;11(6):813–26.

106. Müller HM, Steringer JP, Wegehingel S, Bleicken S, Münster M, Dimou E, et al. Formation of Disulfide Bridges Drives Oligomerization, Membrane Pore Formation, and Translocation of Fibroblast Growth Factor 2 to Cell Surfaces *. J Biol Chem. 2015 Apr 3;290(14):8925–37.

107. Dimou E, Cosentino K, Platonova E, Ros U, Sadeghi M, Kashyap P, et al. Single event visualization of unconventional secretion of FGF2. J Cell Biol. 2018 Nov 23;218(2):683–99.

108. Zehe C, Engling A, Wegehingel S, Schäfer T, Nickel W. Cell-surface heparan sulfate proteoglycans are essential components of the unconventional export machinery of FGF-2. Proc Natl Acad Sci. 2006 Oct 17;103(42):15479–84.

109. Micheletto YMS, Marques CM, Silveira NP da, Schroder AP. Electroformation of Giant Unilamellar Vesicles: Investigating Vesicle Fusion versus Bulge Merging. Langmuir. 2016 Aug 16;32(32):8123–30.

110. García-Sáez AJ, Ries J, Orzáez M, Pérez-Payà E, Schwille P. Membrane promotes tBID interaction with BCLXL. Nat Struct Mol Biol. 2009 Nov;16(11):1178–85.

111. Almeida PF, Pokorny A. Mechanisms of antimicrobial, cytolytic, and cell-penetrating peptides: from kinetics to thermodynamics. Biochemistry. 2009 Sep 1;48(34):8083–93.

112. Parente RA, Nir S, Szoka FC. Mechanism of leakage of phospholipid vesicle contents induced by the peptide GALA. Biochemistry. 1990 Sep 18;29(37):8720–8.

113. Yandek LE, Pokorny A, Florén A, Knoelke K, Langel U, Almeida PFF. Mechanism of the cell-penetrating peptide transportan 10 permeation of lipid bilayers. Biophys J. 2007 Apr 1;92(7):2434–44.

114. Tamba Y, Yamazaki M. Single giant unilamellar vesicle method reveals effect of antimicrobial peptide magainin 2 on membrane permeability. Biochemistry. 2005 Dec 6;44(48):15823–33.

115. Rathinakumar R, Wimley WC. Biomolecular engineering by combinatorial design and high-throughput screening: small, soluble peptides that permeabilize membranes. J Am Chem Soc. 2008 Jul 30;130(30):9849–58.

116. Gregory SM, Cavenaugh A, Journigan V, Pokorny A, Almeida PFF. A quantitative model for the all-or-none permeabilization of phospholipid vesicles by the antimicrobial peptide cecropin A. Biophys J. 2008 Mar 1;94(5):1667–80.

117. Gregory SM, Pokorny A, Almeida PFF. Magainin 2 revisited: a test of the quantitative model for the all-or-none permeabilization of phospholipid vesicles. Biophys J. 2009 Jan;96(1):116–31.

118. Fuertes G, García-Sáez AJ, Esteban-Martín S, Giménez D, Sánchez-Muñoz OL, Schwille P, et al. Pores Formed by Baxα5 Relax to a Smaller Size and Keep at Equilibrium. Biophys J. 2010 Nov 3;99(9):2917–25.

119. Šachl R, Čujová S, Singh V, Riegerová P, Kapusta P, Müller HM, et al. Functional Assay to Correlate Protein Oligomerization States with Membrane Pore Formation. Anal Chem. 2020 Nov 17;92(22):14861–6.

120. Sengupta D, Leontiadou H, Mark AE, Marrink SJ. Toroidal pores formed by antimicrobial peptides show significant disorder. Biochim Biophys Acta. 2008 Oct;1778(10):2308–17.